[AMERICAN JOURNAL OF SCIENCE, VOL. 298, JUNE, 1998, P. 499–533]

DEDUCING GROWTH MECHANISMS FOR MINERALS FROM THE SHAPES OF CRYSTAL SIZE DISTRIBUTIONS

D. D. EBERL*, V. A. DRITS**, and J. ŚRODOŃ***

ABSTRACT. **Crystal size distributions (CSDs) of natural and synthetic samples are observed to have several distinct and different shapes. We have simulated these CSDs using three simple equations: the Law of Proportionate Effect (LPE), a mass balance equation, and equations for Ostwald ripening. The following crystal growth mechanisms are simulated using these equations and their modifications: (1) continuous nucleation and growth in an open system, during which crystals nucleate at either a constant, decaying, or accelerating nucleation rate, and then grow according to the LPE; (2) surface-controlled growth in an open system, during which crystals grow with an essentially unlimited supply of nutrients according to the LPE; (3) supply-controlled growth in an open system, during which crystals grow with a specified, limited supply of nutrients according to the LPE; (4) supply- or surface-controlled Ostwald ripening in a closed system, during which the relative rate of crystal dissolution and growth is controlled by differences in specific surface area and by diffusion rate; and (5) supply-controlled random ripening in a closed system, during which the rate of crystal dissolution and growth is random with respect to specific surface area. Each of these mechanisms affects the shapes of CSDs. For example, mechanism (1) above with a constant nucleation rate yields asymptotically-shaped CSDs for which the variance of the natural logarithms of the crystal sizes (β^2) increases exponentially with the mean of the natural logarithms of the sizes (α). Mechanism (2) yields lognormally-shaped CSDs, for which β^2 increases linearly with α, whereas mechanisms (3) and (5) do not change the shapes of CSDs, with β^2 remaining constant with increasing α. During supply-controlled Ostwald ripening (4), initial lognormally-shaped CSDs become more symmetric, with β^2 decreasing with increasing α. Thus, crystal growth mechanisms often can be deduced by noting trends in α versus β^2 of CSDs for a series of related samples.**

INTRODUCTION

Crystal size distributions (size versus frequency plots, or CSDs) of minerals often have distinctive shapes which can convey information about crystal growth history (Wagner, 1961; Baronnet, 1982). A CSD first develops during nucleation, when crystals with sizes equal to or greater than that of the critical nucleus appear and grow in highly supersaturated solutions. If solution supersaturation falls to a level at which nucleation ceases, the CSD may continue to evolve by open system crystal growth without additional nucleation. The kinetics for this growth will be controlled either by how fast the crystal's surface grows given an essentially infinite supply of nutrients (surface-controlled growth kinetics) or may be limited by the rate at which nutrients reach the growing surface (supply-controlled kinetics). As supersaturation approaches equilibrium, less stable crystals may dissolve, yielding material for other crystals of the same phase to grow during a ripening process, thereby again modifying the shape of the CSD. Finally, crystals also may grow by agglomeration with other crystals, without significant dissolution.

Attempts to model crystal nucleation and crystal growth from classical kinetic theory have been disappointing (Ohara and Reid, 1973; Mullin, 1974; Dowty, 1980; Kirkpatrick, 1981; Lasaga, 1982). Some workers have abandoned such models altogether in favor of a chemical engineering approach that uses empirical methods, developed from the measurement of CSDs for crystals grown in industrial crystallizers, to describe nucleation and growth rates for minerals (Randolph and Larson, 1971;

* United States Geological Survey, 3215 Marine Street, Boulder, Colorado 80303-1066
** Institute of RAN, Pyzevskij per. D. 7, 109017 Moscow, Russia
*** Institute of Geological Sciences PAN, Senacka 1, 31002 Krakow, Poland

Marsh, 1988; Cashman and Marsh, 1988; Cashman and Ferry, 1988). This approach has been criticized because it fails to generate the detailed shapes of CSDs for many systems, particularly over the smaller size ranges (Larson and others, 1985; Garside and others, 1976; Kerrick and others, 1991). A quantitative theory for Ostwald ripening (the LSW theory of Lifshitz and Slyozov, 1961, and Wagner, 1961), although theoretically sound, also is less than satisfactory in practice because predicted shapes for CSDs for ripened minerals often do not fit actual measurements (Chai, ms and 1975; Colbeck, 1986; Eberl and others, 1990; Inoue and Kitagawa, 1994).

This paper presents numerical methods to simulate crystal growth and thereby to predict the shapes of CSDs that result from several crystal growth mechanisms. These shapes can then be used to deduce geologic history from measured CSDs for minerals.

THEORY

The lognormal distribution.–The development of this method for simulating crystal growth was inspired by the observation that the shapes of CSDs for many (although not all) crystalline substances are approximately lognormal (Eberl and others, 1990). A lognormal distribution is a distribution in which the logarithms of the observations (that is, particle sizes) are normally distributed. For example, CSDs for several mineral samples taken from the literature are fitted with lognormal curves in figure 1. The Chi-square test (Krumbein and Graybill, 1965), which was used to compare theoretical and simulated distributions with measured distributions, indicates that, for five out of the six samples given in the figure, there is no reason to reject the hypothesis that the curves are the same at a high significance level (>10 to >20 percent; see table 1). Generally, the deviation between theoretical or simulated and measured distributions is considered to be due solely to statistical fluctuations if the significance level is >1 to >5 percent (Exner and Lukas, 1971). Only the CSD for the sphene sample (fig. 1D) fails this stringent test (significance level <1 percent; table 1). Its mode is shifted slightly to the right with respect to the theoretical lognormal curve.

When CSDs are lognormal, they are described by the equation:

$$g(X) = \left[\frac{1}{X\beta\sqrt{2\pi}}\right] \exp\left\{-\left(\frac{1}{2\beta^2}\right)[\ln(X) - \alpha]^2\right\}, \quad (1)$$

where g(X) describes the theoretical lognormal distribution of X (Krumbein and Graybill, 1965). If f(X) is the observed frequency of crystal dimension X, then alpha (α) describes the mean of the logarithms of the crystal dimension:

$$\alpha = \Sigma \ln(X) f(X); \quad (2)$$

and β^2 describes the variance of the logarithms of the crystal dimension:

$$\beta^2 = \Sigma[\ln(X) - \alpha]^2 f(X). \quad (3)$$

Thus a theoretical lognormal distribution can be calculated if the two experimental parameters α and β^2 are known: α is a function of the mean size, and β^2 is a function of the shape or uniformity of the distribution.

If instead of X, another independent variable parameter, $u = X/\overline{X}$ is used, and $\overline{X}$ is the mean crystal dimension, then the so-called reduced lognormal distribution has the form:

$$g(u) = \frac{1}{\beta u\sqrt{2\pi}} \exp\left[-\frac{(\ln(u) + \beta^2/2)^2}{\beta^2}\right]. \quad (4)$$

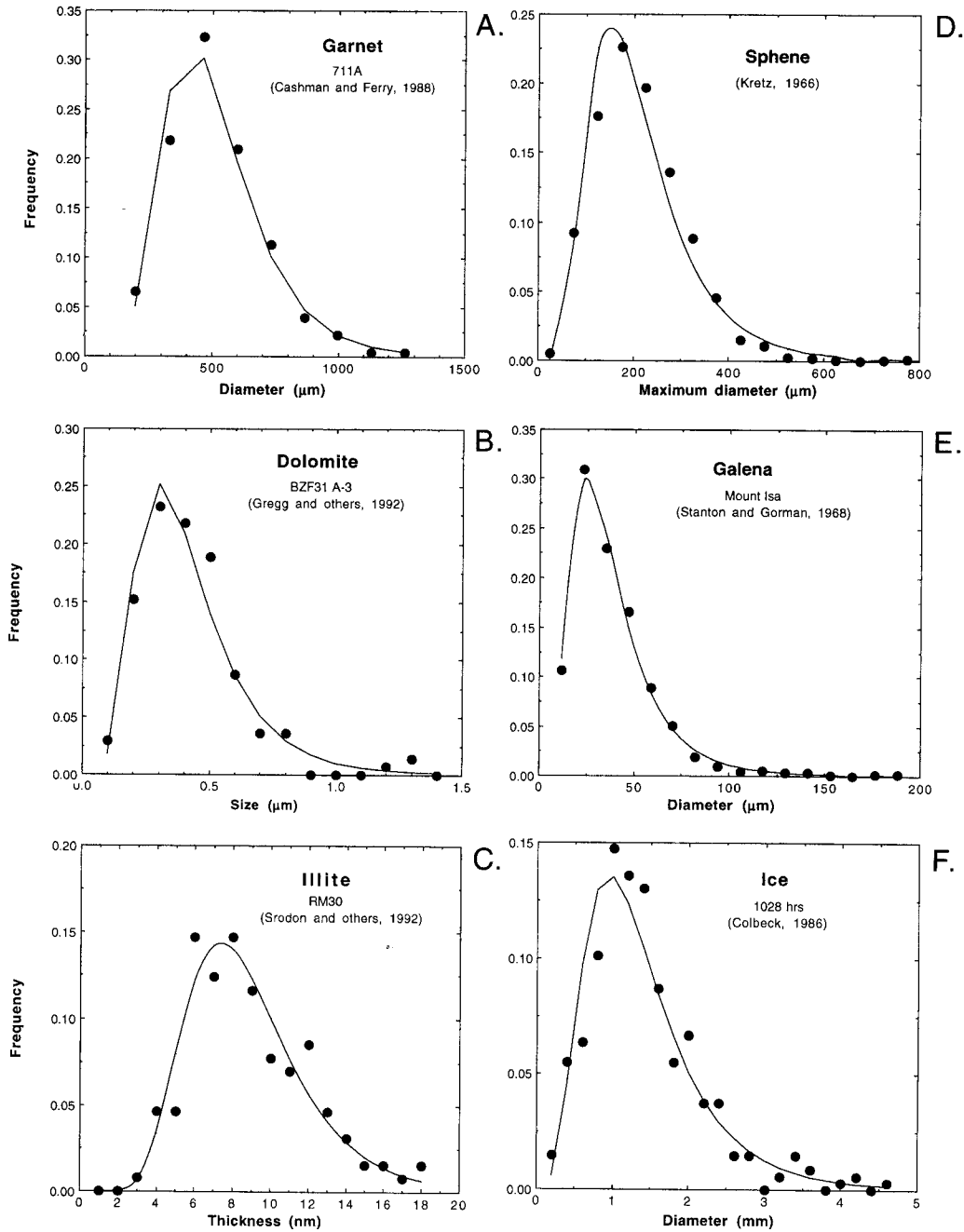

Fig. 1. Particle size data from the literature (points), with superimposed theoretical lognormal curves calculated from these data (solid lines).

This distribution is independent of α-values; therefore, to specify the reduced theoretical lognormal distribution of u one need know only one parameter, β^2. In comparing plots of two or more non-lognormal distributions that have different bin sizes (that is, different data groupings), it is convenient to divide the frequencies for each

TABLE 1

Chi-square analysis of CSDs presented in the figures

Fig. No.	Observed Distribution// Expected Distribution	Chi^2 Value	Degrees Freedom	Significance Level (Percent)
1	Garnet//Lognormal	1.30	6	>20
	Dolomite//Lognormal	10.09	7	10 to 20
	Illite//Lognormal	12.77	9	10 to 20
	Sphene//Lognormal	411.41	10	<1
	Galena//Lognormal	9.78	10	>20
	Ice/Lognormal	11.91	12	>20
2	3 cycles//Lognormal	27.71	4	<1
	5 cycles//Lognormal	25.8	13	1 to 5
	7 cycles//Lognormal	32.16	30	>20
4	A. 200 crystals per cycle//Lognormal	55.62	8	<1
	B. Decaying nucleation//Lognormal	12.88	13	>20
	C. Accelerating nucleation//Lognormal	152.1	9	<1
5	A. Overgrowth of 4A//Lognormal	52.11	23	<1
	B. Overgrowth of 5A//Lognormal	21.32	24	>20
6	A. Mean = 7.5//Lognormal	17.02	14	>20
	A. Mean = 50//Lognormal	22.29	17	10 to 20
	A. Mean = 100//Lognormal	29.18	19	5 to 10
8	A. Open system to 7.7-mean//Lognormal	25.69	14	2.5 to 5.0
	B. Ripened fraction 0.05//Lognormal	316.14	16	<1
11	A. Mean = 7.7//Lognormal	17.02	14	>20
	B. Mean = 9.5//Lognormal	23.18	22	>20
13	A. Phlogopite//GALOPER simulation	31.83	7	<1
	B. GALOPER simulation//Le Puy	61.29	15	<1
15	A. Zempleni//Lognormal	0.86	7	>20
	A. GALOPER simulation//Zempleni	8.07	7	>20
	B. RM35A//Lognormal	1.39	8	>20
	B. GALOPER simulation//RM35A	21.33	13	5 to 10
	C. RM30//Lognormal	0.89	10	>20
	C. GALOPER simulation//RM30	25.79	21	>20
	D. AR1R//Lognormal	0.69	30	>20
	D. GALOPER simulation//AR1R	23.24	40	>20
17	A. BZF31A-3//Lognormal	11.25	8	10 to 20
	B. BZF31C-6//Lognormal	10.72	10	>20
	C. BZF31C-9//Lognormal	6.65	10	>20
	D. BZF31E-13//Lognormal	4.74	11	>20
18	A. Fisher calcite//Lognormal	2.34	9	>20
	B. GALOPER simulation//Calcite ripened 25 h	13.5	16	>20
	C. GALOPER simulation//Calcite ripened 336 h	9.65	6	10 to 20
	D. GALOPER simulation//Calcite ripened 1008 h	8.99	9	>20

distribution by the maximum frequency of that distribution. Then, reduced plots (frequency/maximum frequency plotted versus size/mean size) will coincide if the shapes of the distributions are the same. If reduced distributions coincide, they are said to have a steady-state shape.

Generation of lognormal CSDs by the Law of Proportionate Effect (LPE).–We are aware of only one way to generate a lognormal distribution by growth of linear crystal sizes and that is by the Law of Proportionate Effect (LPE; Kapteyn, 1903; Koch, 1966, 1969). According to the central limit theorem, the familiar normal (bell-shaped or Gaussian) distribution can be generated by addition of small, independent, random variables to a quantity. Crystal growth can not be governed by such a random process because CSDs are poorly represented by normal distributions (Randolph and Larson, 1988). A lognormal distribution can be generated similarly by adding such random variables to the logarithm of a quantity. However, during crystal growth we are measuring the growth of a specific linear dimension in a crystal and not its logarithm. Therefore, the lognormal distribution needs to be generated directly from growth of the crystal's dimension.

As is demonstrated in app. 1, the lognormal distribution is generated directly by the equation for the LPE:

$$X_{j+1} = X_j + \epsilon_j X_j, \tag{5}$$

where, for this discussion of crystal growth, X_j is some specified dimension in a crystal, and ϵ_j is a small, randomly varied number. The form of the distribution of ϵ_j's is irrelevant to the final distribution as long as ϵ_j varies independently from X_j. X_{j+1} is the new crystal dimension after one calculation cycle. In terms of crystal growth, the equation states that the rate of growth (per calculation cycle) will depend on the crystal's previous size times the system's variability (ϵ_j). The system's variability, which includes factors such as thermal and chemical fluctuations or heterogeneities, the presence of favorable growth sites on surfaces, the surface area and energy of crystals, the diffusion rate, the porosity and permeability, et cetera, all of which may be treated independently in microscopic models for crystal growth, here is condensed into a random number allowed to vary between zero and one. This range for ϵ_j was chosen because it works for simulating CSDs for natural and synthetic systems.

Other methods to simulate crystal growth.–The lognormally-shaped distributions in figure 1 can be modeled similarly by the gamma function (Vaz and Fortes, 1988; Randolph and Larson, 1988). CSDs having these shapes can be simulated by a cell model in which randomly distributed grains nucleate simultaneously and grow at a constant, isotropic rate, thereby leading to a Voronoi partition of space (Vaz and Fortes, 1988; Weaire and others, 1986). Other approaches use cellular or Johnson-Mehl simulations (Mahin and others, 1980; Frost and Thompson, 1987) and spiral growth or surface nucleation growth (Nielson, 1964; Nordeng and Sibley, 1966). These and other models that assume constant growth rates (Joesten, 1991; Kerrick and others, 1991) fail to simulate size dependent growth and growth dispersion (discussed below), processes that have been observed in crystal growth experiments. Therefore they do not adequately describe crystal growth in many real systems.

Size dependent growth and growth dispersion.–Crystals of different sizes may grow at different rates, even though they exist in the same supersaturated solution. During this type of growth, large crystals almost always grow faster than small crystals (Mullin, 1974; Randolph and Larson, 1988). Also, crystals that initially have the same size and that sit side by side in the same solution may grow at different rates (White and Wright, 1971; Randolph and White, 1977; Jancic and others, 1984; Randolph and Larson, 1988). These processes, termed size dependent growth and growth dispersion, are embodied in the LPE (eq 5). Such processes may occur in natural systems. Nordeng and Sibley (1966), from a study of cathode luminescent zones in ancient dolomite crystals, conclude that the growth rate equation is $dr/dt = kr$, where r is the crystal radius, t is time, and k is the rate coefficient. They indicate that the observed dependence of growth rate on crystal radius could result from spatial variations in k. Thus their empirically determined growth rate (kr) is analogous to that found in the LPE ($\epsilon_j X_j$).

The chemical reasons for size dependent growth and growth dispersion are unclear, but there has been speculation that size dependent growth could result from a greater proportion of defects on the surfaces of larger crystals, leading to an increase in average growth rate (Garside and others, 1976). However, if the LPE is the governing crystal growth law, then it is unlikely that a study of microscopic growth processes for individual crystals will improve predictions for the evolution of CSDs. The variable in eq (5) that drives growth is a random number, indicating complex interactions not easily described by simple mechanisms.

CRYSTAL GROWTH IN OPEN SYSTEMS

An open system is defined here as a system in which matter is supplied to the growing crystals by a source other than the phase under study. In other words, material is

being added to the crystalline phase. As an example, the growth in a sealed capsule of a crystalline phase from an amorphous phase would be considered to be an open system with respect to the crystalline phase until the amorphous phase is completely consumed. In a closed system, some of the crystalline phase itself dissolves to supply material to other crystals of the same phase that are growing during a ripening process; therefore, the mass of the mineral is conserved.

Surface-controlled growth in the open system.–The rate of crystal growth may be limited either by the rate of supply of nutrient ions to the crystal surface, which is known as supply- or transport-controlled growth (often diffusion limited), or by the growth kinetics of the crystal itself, which is known as interface- or surface-controlled growth (Berner, 1981). In this section it is assumed that the crystals can grow as fast as is required by the LPE (eq 5) and are not limited by the supply of nutrients.

A computer program named GALOPER (Growth According to the Law of Proportionate Effect and by Ripening) was written in Microsoft Excel[1] macro language to carry out these and subsequent calculations. Eq (5) was iterated for 1001 crystals for a specified number of cycles, and the lognormal parameters α and β^2 for the resulting distribution were calculated from eqs (2) and (3). A theoretical lognormal distribution then was calculated from these parameters (eq 1), and this distribution was compared with the GALOPER calculated distribution using the Chi-square test (table 1). A summary of crystal growth mechanisms and their characteristics, deduced form GALOPER calculations, is given in table 2.

Starting with 1001 crystals having a diameter of 1 nm, figure 2 shows the generation of crystal size distributions by the LPE for 3, 5, and 7 calculation cycles. The solid curves are the theoretical lognormal distributions, which are closely matched by the calculation (symbols). In accordance with the theory discussed in app. 1, figure 2 and table 1 indicate that open system growth by surface control is distinguished by two properties: (1) convergence to a lognormal distribution of the CSD as the number of calculation cycles increases (the significance level for the Chi-square test increases from <1 percent to a range between 1 and 5 percent to >20 percent with increasing number of cycles; table 1); and (2) an increase in variance (β^2) with increasing mean. As the mean diameter increases from 3.4 to 7.5 to 16.9 nm (fig. 2), β^2 increases from 0.12 to 0.20 to 0.26, respectively.

The mean size ($\overline{X}_n$) of a CSD after a given number of calculation cycles (n) is related to the initial mean size ($\overline{X}_0$) and the mean variability ($\bar{\epsilon}$, which is equal to the mean variation for ϵ in eq 5). From eq (A8) in app. 1:

$$\overline{X}_n = \overline{X}_0(1 + \bar{\epsilon})^n. \quad (6)$$

This relationship, true for open system, surface-controlled growth, is demonstrated in figure 3, curve 1.

Simultaneous nucleation and growth.–It was assumed above that all the crystals start with the same crystal diameter (for example, 1 nm) and then grow according to the LPE (eq 5). This assumption may be unrealistic for some systems, because crystals may nucleate at the same time as previously nucleated crystals are growing. Unless nucleation is very rapid, purely open system growth may begin with a range of crystal sizes inherited from such a nucleation and growth step.

GALOPER simulates three types of continuous nucleation and growth mechanisms: the first having a constant nucleation rate, and the others having decaying or accelerating nucleation rates. The first mechanism should apply to a system in which nutrients are continually entering a reacting volume at a constant rate, for example, by groundwater flow or by dissolution of unstable phases. A decaying nucleation rate may

[1]Trade names are used for identification purposes only and do not constitute endorsement by the United States Geological Survey.

TABLE 2

Summary of crystal growth mechanisms and their characteristics

System	Growth Mechanism	CSD Shape	Comments
Open	Nucleation and growth with constant or accelerating nucleation rate.	Asymptotic.	β^2 increases exponentially with increase in α.
	Nucleation and growth with decaying nucleation rate.	Lognormal.	β^2 increases linearly with increase in α.
	Surface-controlled growth.	Lognormal.	β^2 increases linearly with increase in α.
	Supply-controlled growth.	Preserves shape of previous CSD.	β^2 remains constant with increase in α; therefore, steady-state reduced profiles.
Closed	Ostwald ripening (supply-controlled).	CSD becomes more symmetrical with increasing percentage of ripening, becomes negatively skewed, and eventually approaches universal steady-state reduced profile.	Distribution maximum moves to the right of theoretical lognormal curve. Generally, β^2 decreases with increase in α. Universal steady-state profile may not be reached.
	Random ripening (supply-controlled). Also termed non-Ostwald or kinetic ripening.	Preserves shape of previous CSD.	A large amount of material passes through solution for a small increase in mean size. β^2 remains constant with increase in α; therefore steady-state reduced profiles.
	Agglomeration.	Can be pseudo-lognormal or multimodal, or have other shapes.	Very little material need pass through solution for a large increase in mean size. If most of the crystals are involved, β^2 may decrease; otherwise it may increase.

apply, for example, to an enclosed volume in which one or more essential mineral nutrients are limited and become depleted as nucleation and growth proceeds. Accelerating nucleation may occur, for example, during the cooling of molten rock.

For the constant nucleation rate simulation, the calculations assume that a specified number of crystals having a specified diameter for the critical nucleus appear during each calculation cycle and then grow according to the LPE during subsequent calculation cycles. Nucleation ceases when approx 1000 crystals have nucleated. Growth according to the LPE leads to a pure lognormal distribution, the shape of which is altered each time new crystals are added to the system during nucleation. The lognormal shape may be recovered approximately by surface-controlled open system growth after nucleation has ceased.

Crystals having a critical nucleus diameter of 2.0 nm were nucleated at a constant rate and grown in the GALOPER program with a nucleation rate of 200 crystals per cycle (fig. 4A). This calculation yielded a mean diameter of 5.2 nm and an asymptotic shape for the CSD typical for this type of growth mechanism. A theoretical lognormal distribution calculated from the same data, presented as a solid line in the figure, fails the Chi-square test (table 1), indicating that the lognormal curve differs significantly from the calculated asymptotic CSD.

The approximate mean size after the nth calculation cycle ($\overline{X}_n$) for nucleation and growth with a constant nucleation is given by:

$$\overline{X}_n = \frac{\overline{X}_0}{n\bar{\epsilon}}[(1 + \bar{\epsilon})^n - 1]. \quad (7)$$

This equation is plotted in figure 3, curve 2.

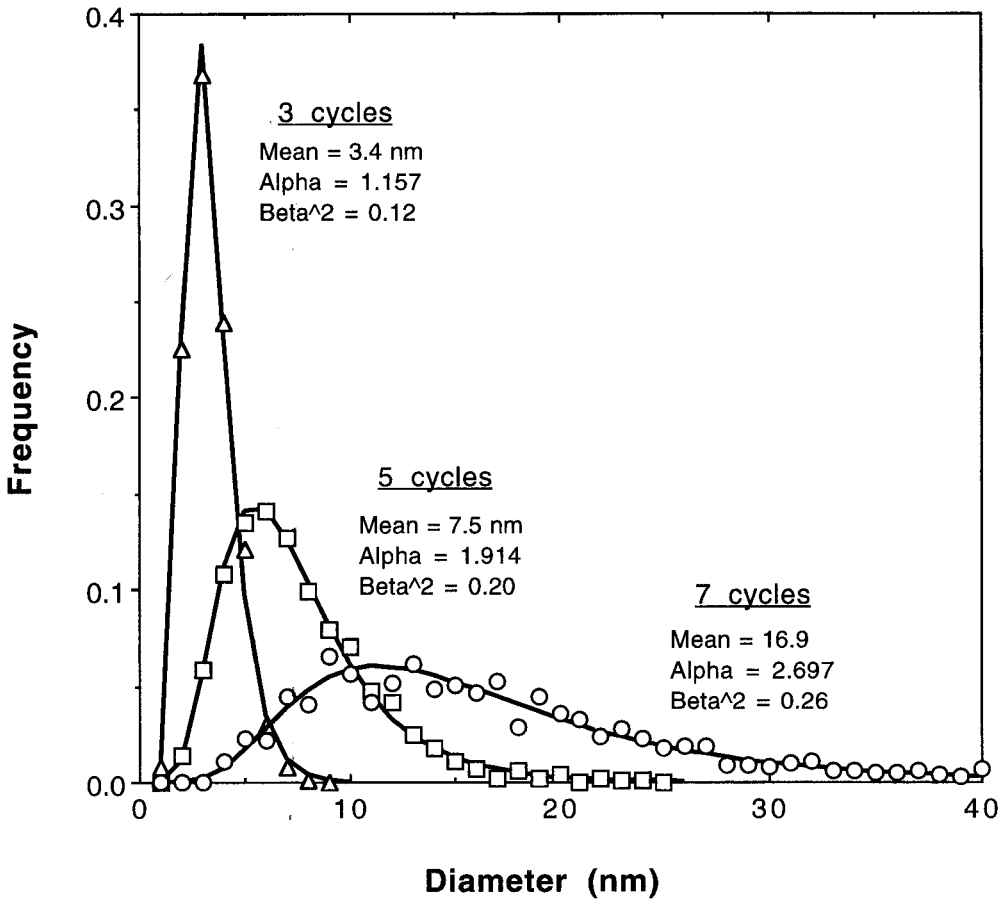

Fig. 2. GALOPER-calculated CSDs (symbols) for surface-controlled open system growth, using 3, 5, and 7 calculation cycles (eq 5) and an initial crystal diameter of 1 nm, compared with theoretical lognormal curves calculated from these data (solid lines).

The simulation with a decaying nucleation rate assumes that the reacting volume has the potential to nucleate and grow 1001 crystals. Random numbers that vary between 0 and 1 are assigned to each virtual crystal, and a probability for nucleation is entered into the program. If, for example, the entered probability is 0.5, then during the first calculation cycle all virtual crystals having a random number less than 0.5 (approx 500 crystals) will nucleate. During the second calculation cycle, new random numbers are assigned to the approx 500 remaining virtual crystals, approx 250 more crystals will nucleate, and all of the previously formed crystals (approx 500) then grow one cycle according to the LPE and so on until all 1001 crystals have nucleated. Crystals (2.0 nm) were nucleated and grown using a decaying nucleation rate with a probability for nucleation of 0.9 (fig. 4B). This calculation yielded a mean diameter of 6.5 nm. The shape of the CSD for this process is dominated by LPE growth during the last phases of nucleation, and therefore the CSD is lognormal (table 1).

Simulation with an accelerating nucleation rate assumes that nucleation rate follows the arbitrarily chosen formula: number of crystals nucleating per calculation cycle = exp (kn), where k is a constant, and n is the calculation cycle number. If k = 0.55, the

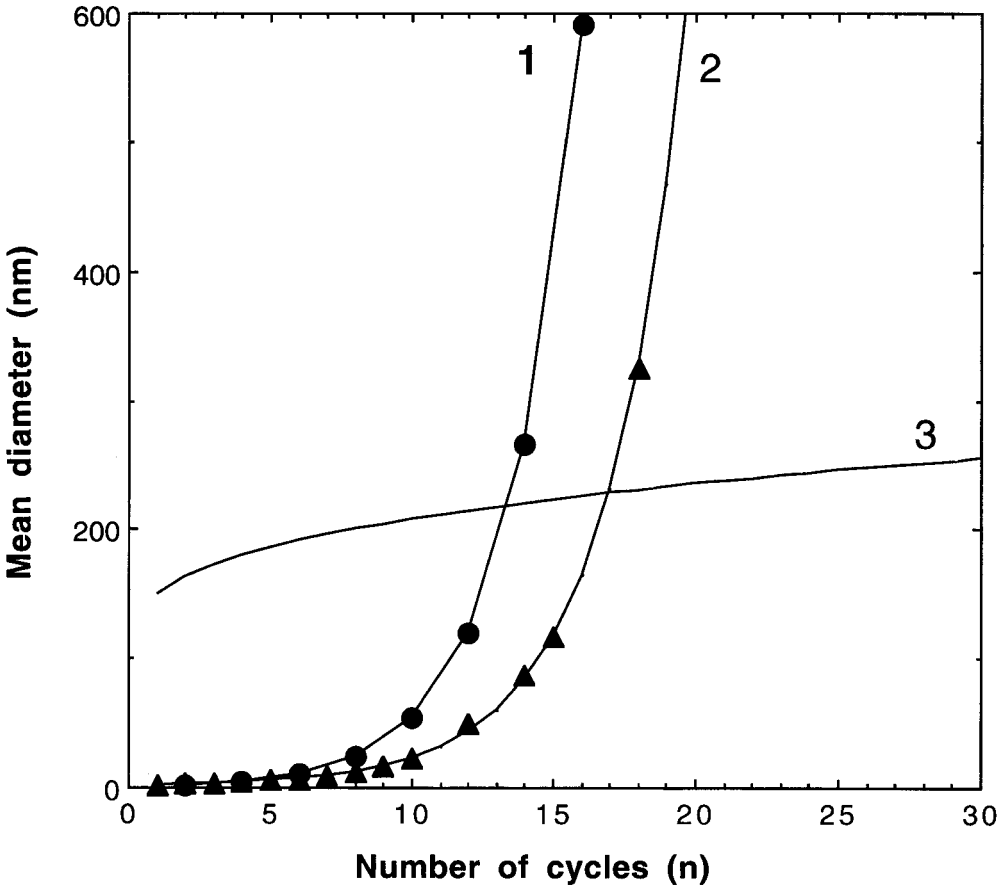

Fig. 3. Plots of rate equations (solid curves) for: (1) surface-controlled open system growth (eq 6 in text) starting with 2 nm crystals; (2) constant-rate nucleation and growth (eq 7 in text) starting with 2 nm crystals; and (3) supply-controlled growth (eq 9 in text) starting with a mean size of 100 nm and using k = 50. Epsilon was allowed to vary between 0 and 1 for all calculations (that is, $\bar{\epsilon} = 0.5$). The symbols represent GALOPER calculations for the corresponding growth mechanisms.

CSD based on approx 1000 crystals (fig. 4C) is very similar to that found for constant nucleation and growth (fig. 4A), except that the variance is greater for a given mean. The CSD is not lognormal (table 1).

Overgrowth of previously nucleated crystals.–The asymptotic CSD in figure 4A was overgrown using the surface-controlled open system growth mechanism in GALOPER to test if the LPE can produce a lognormal distribution from a CSD that is not lognormal. Starting with a mean diameter of 5.2 nm (fig. 4A), progressive overgrowth yielded mean diameters of 17.7 nm (fig. 5A) and 89.8 nm (fig. 5B). The smaller amount of overgrowth produced a CSD that is pseudo-lognormal (which means that the significance level is <1 percent, although it appears lognormal-like by inspection; table 1) and that has a small pointed hat (here termed a "circumflex" after the French accent) that extends above the mode of the theoretical lognormal curve. The circumflex decreases in size as the amount of overgrowth increases, and the shape of the CSD approaches that of the theoretical lognormal curve, with the Chi-square test significance level increasing to >20 percent (table 1).

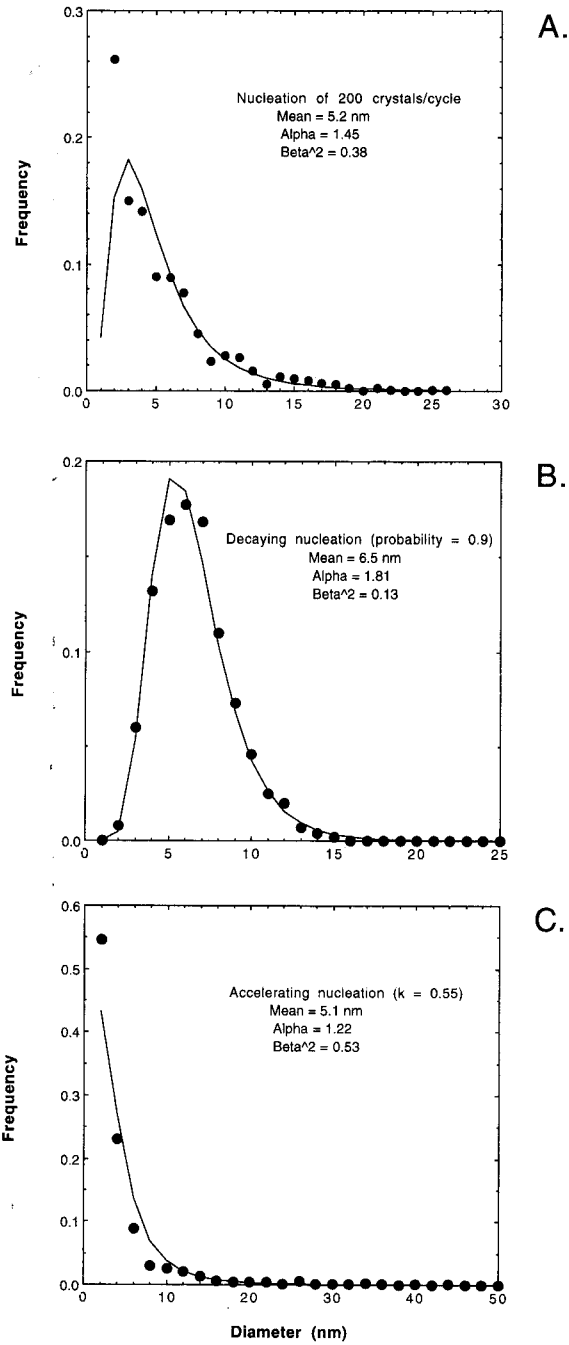

Fig. 4. GALOPER-calculated CSDs (points) for the continuous nucleation and growth mechanism assuming nucleation having: (A) a constant rate; (B) a decaying rate; and, (C) an accelerating rate. Critical nucleus size = 2.0 nm. The solid lines are lognormal fits to the data.

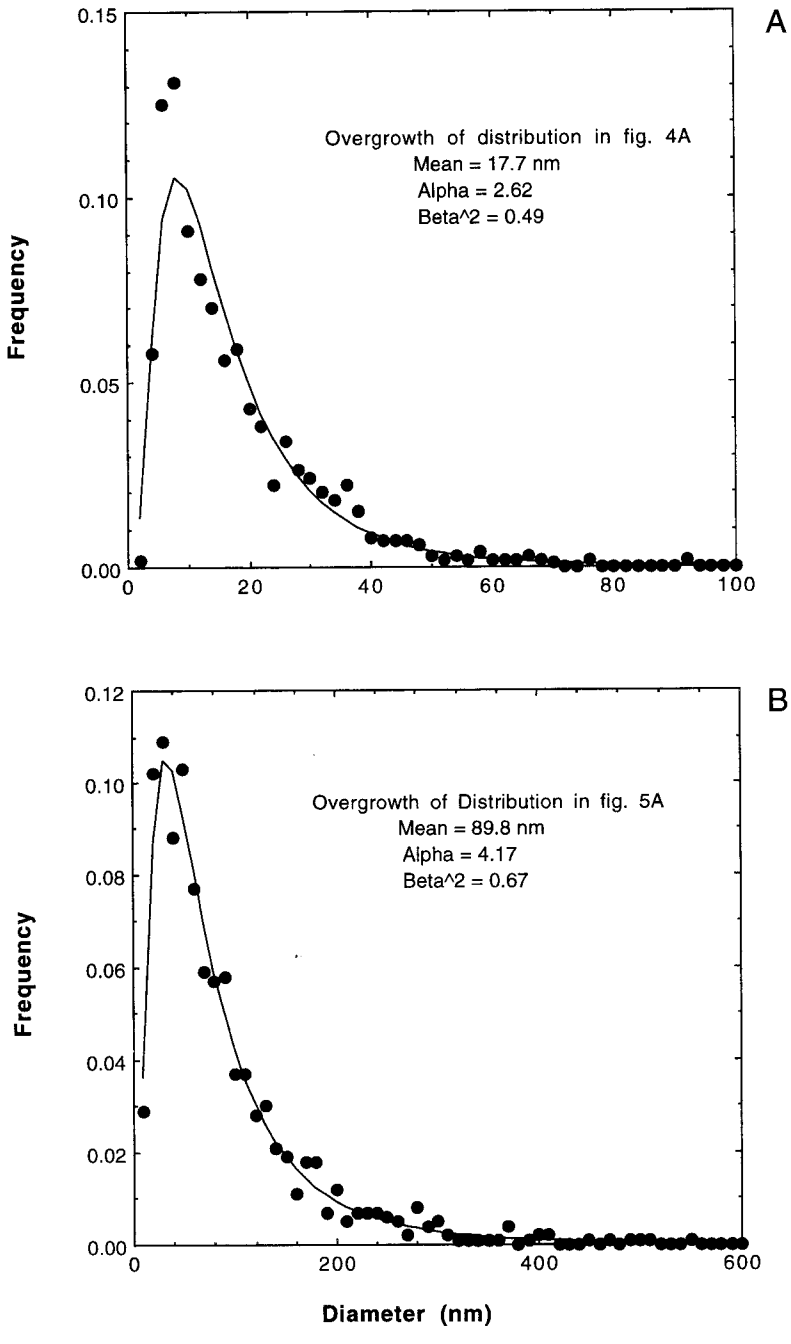

Fig. 5. GALOPER-calculated CSDs (points) for overgrowth of previously formed CSDs by surface-controlled open system growth. (A) = overgrowth of CSD in figure 4A; (B) = overgrowth of distribution in (A). The solid lines are lognormal fits to the data.

Supply-controlled growth in the open system.–One can imagine an open system in which the rate of crystal growth is controlled by the rate of nutrient supply rather than by the rate at which the crystal surface can grow in an infinite reservoir of nutrients. For example, the supply may be slowed by diffusion or by the rate of dissolution of an unstable phase that is a nutrient source, or crystals may grow so large that supply can not keep up with the exponentially increasing demand for nutrients required by LPE growth. This situation is simulated in GALOPER by specifying the total increase in volume that 1001 crystals are permitted ($\Sigma\Delta V_a$) during each cycle of eq (5). The crystals first are allowed to grow freely during a calculation cycle according to eq (5). Next the growth volume for that cycle for each crystal is calculated ($\Delta V_{j,LPE}$), and the growth volumes for all crystals are summed ($\Sigma\Delta V_{j,LPE}$). The unconstrained growth volume for each crystal then is reduced proportionately by the ratio of allowed volume to unconstrained growth volume:

$$\Delta V_j = (\Delta V_{j,LPE})\frac{\Sigma\Delta V_a}{\Sigma\Delta V_{j,LPE}}. \quad (8)$$

The corrected growth volume for each crystal (ΔV_j) is added to the previous volume of the crystal, and a new diameter for each crystal for that growth cycle is then calculated from the equation for the volume of a sphere. The calculation is repeated for each growth cycle. Therefore, during this type of growth the LPE is still the growth law, but growth is limited proportionately by supply.

Supply-controlled open system growth is one of two growth mechanisms that does not have a distinctive CSD shape (the other being random ripening); rather, it adopts the shape of an existing CSD. In figure 6A, a previously formed, GALOPER-calculated CSD having a lognormal shape, a mean crystal diameter of 7.5 nm, a $\beta^2 = 0.21$, and a total initial system volume of 3.52×10^5 nm^3 for 1001 crystals, is overgrown using a constant volume added ($\Sigma\Delta V_a$ in eq 8). For each cycle $\Sigma\Delta V_a = 10^5$ nm^3, to yield lognormal CSDs (table 1) having means of 50 and 100 nm and having approximately the same variance. A similar calculation and result for an asymptotic CSD is shown in figure 7A. The figures indicate that overgrowth of CSDs by this mechanism is distinguished by two properties: (1) the lognormal or asymptotic shapes of the distributions are preserved, and (2) the variance of the CSDs remain constant. If β^2 remains constant with an increase in mean size, then the CSDs have a steady-state shape (figs. 6B and 7B) when plotted on reduced axes (diameter/mean diameter versus frequency/maximum frequency). Previous workers (for example, Eberl and Środoń, 1988; Inoue and others, 1988; Eberl and others, 1990) have incorrectly ascribed the lognormal steady-state shape (fig. 6B) to Ostwald ripening. It will be shown below that Ostwald ripening does develop in the direction of a universal steady-state shape for reduced CSD plots, but that the resulting shape is not lognormal.

The relation for supply-controlled open system growth between the mean size after n calculation cycles ($\overline{X}_n$) and the initial mean radius ($\overline{X}_0$) is:

$$\overline{X}_n = \overline{X}_0 + k(n)^{1/3}, \quad (9)$$

where k is a constant that is proportional to the volume added for each cycle ($\Sigma\Delta V_a$). This equation is plotted in figure 3, curve 3.

CRYSTAL SIZE EVOLUTION IN CLOSED SYSTEMS

Some crystals of a phase must dissolve for other crystals of the same phase to grow in a closed system in which solution composition straddles equilibrium. Two main types of crystal growth mechanisms are simulated here: Ostwald ripening (both supply- and surface-controlled), during which surface free energy tends toward a minimum by

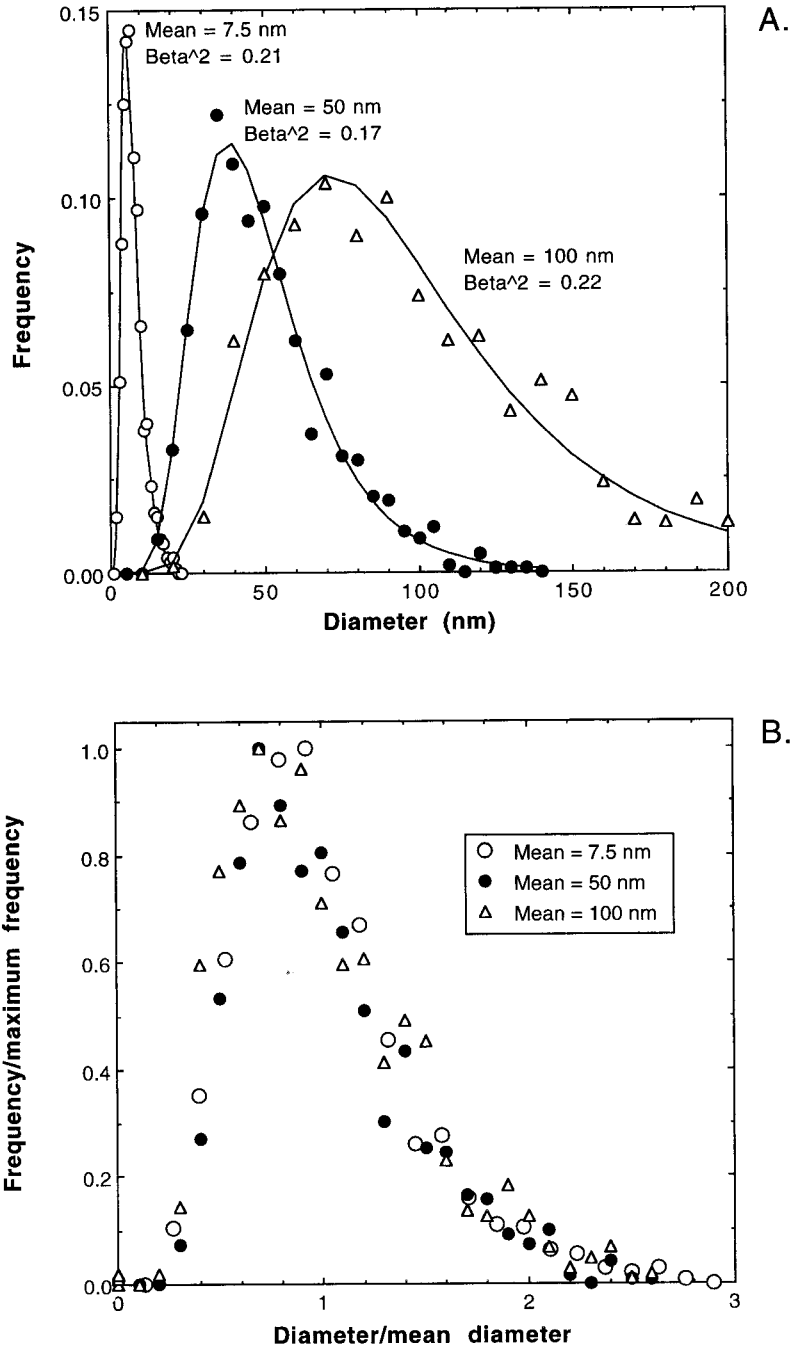

Fig. 6. GALOPER-calculated CSDs for supply-controlled open system overgrowth starting with a lognormal distribution. (A) = overgrowth starting with a lognormal CSD having a mean size of 7.5 nm; (B) = Steady-state reduced plot of CSDs in (A).

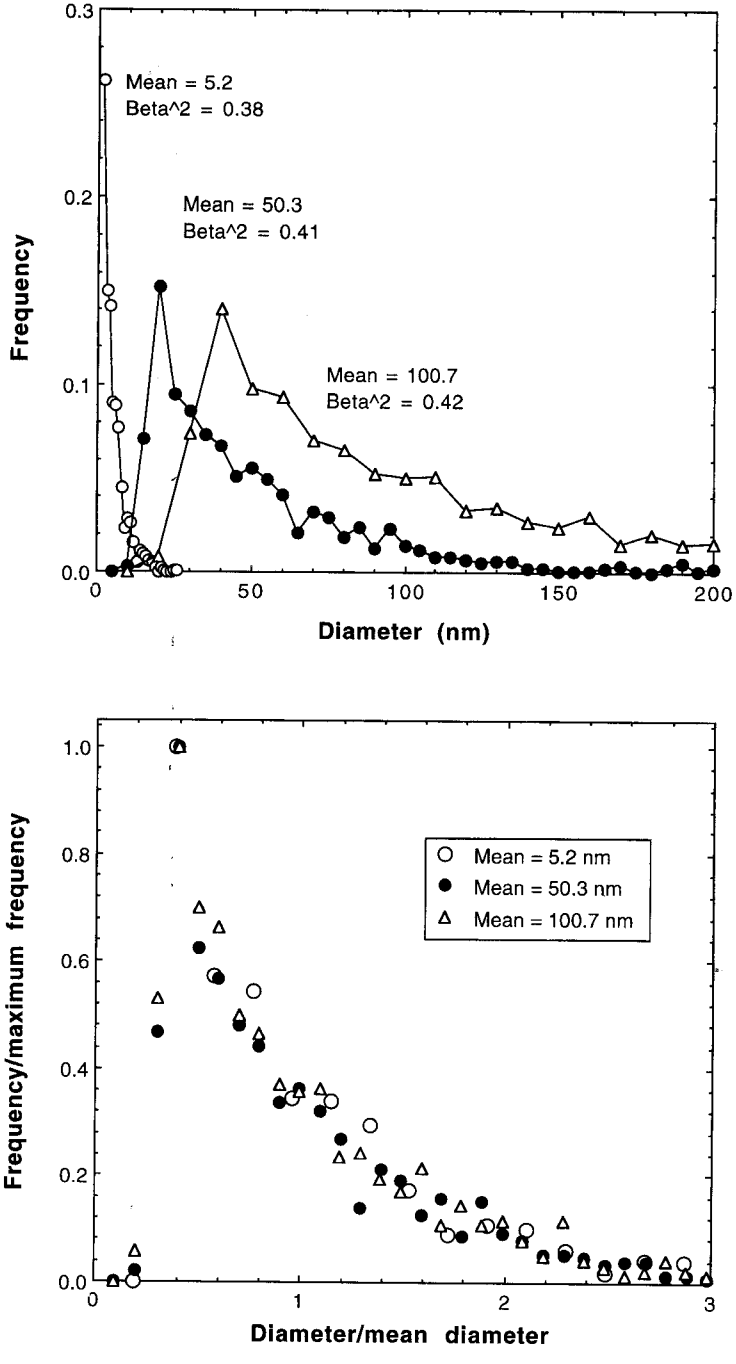

Fig. 7. GALOPER-calculated CSDs for supply-controlled open system overgrowth starting with an asymptotic distribution. (A) = overgrowth starting with an asymptotic CSD having a mean size of 5.2 nm; (B) = Steady-state reduced plot of CSDs in (A).

dissolution of small particles, transport of matter through solution, and growth of large particles (Baronnet, 1982) and supply-controlled random ripening (also called non-Ostwald or kinetic ripening; Söhbel and Garside, 1992), in which some property of the system other than crystal size determines crystal stability during a ripening process. Possible properties include crystal defect density, chemical composition, structural heterogeneity, strain, or environmental heterogeneity. A third type of crystal growth mechanism, crystal agglomeration, will be discussed briefly. This occurs when crystals grow together to produce suddenly much larger crystals.

Ostwald ripening.–During Ostwald ripening, the smaller particles (which have the largest specific surface free energy) dissolve while the larger particles grow larger. Crystals of intermediate size that neither dissolve nor grow are in true equilibrium with solution and are said to have the critical radius (r*). Because the system continues to lose fine particles with time and because the level of supersaturation is influenced by the solubility of the finest particles, the level of supersaturation during ripening continues to fall. Therefore the size of the critical radius increases with time. As long as there is a distribution of particle sizes in the system, ripening never ceases. However, as mean crystal size increases, the differences in specific surface free energy decrease, and an initially rapid evolution of the CSD may become so slow as to be negligible.

The GALOPER program uses the equations given by Markworth (1970) for diffusion- (supply-) and surface- (interface-) controlled Ostwald ripening. These equations are based on the LSW theory for ripening of Lifshitz and Slyozov (1961) and Wagner (1961). A more detailed description of the theoretical approach is given in app. 2. For diffusion-controlled ripening, the instantaneous rate at which a crystal changes size is given by:

$$\frac{dr}{dt} = \frac{K}{r}\left(\frac{1}{r^*} - \frac{1}{r}\right), \tag{10}$$

where r = the crystal radius, t = time (or calculation cycles), r* = the critical radius, which is equal to the mean radius ($\bar{r}$), and K is a constant (see app. 2).

A similar equation is given for surface- (interface-) controlled ripening:

$$\frac{dr}{dt} = K'\left(\frac{1}{r^*} - \frac{1}{r}\right), \tag{11}$$

where K′ is a constant, and $r^* = \overline{r^2}/\bar{r}$ = volume-weighted mean radius, where the bars refer to mean values. The equation for supply-controlled ripening probably is closer to reality than that for surface-controlled ripening, because crystals that dissolve during ripening appear to be rounded rather than etched (Loveland and Trivelli, 1947; Chai, ms and 1975; Baronnet, 1974; Colbeck, 1986). This morphology is indicative of dissolution by supply-(transport-) control (Berner, 1981); therefore, growth kinetics also are likely be supply-controlled. Walton (1967) also indicates that ripening is a diffusion- (supply-) controlled process. GALOPER calculations also favor the supply-control endmember, because CSDs calculated for ripening by surface control do not fit actual measurements.

In the GALOPER program, a CSD is first calculated in the open system. Then an arbitrary K (or K′) is entered into the closed-system part of the program that yields a rate of crystal growth that is sufficiently rapid for ripening to proceed at a convenient rate. After each calculation cycle, which corresponds to one iteration of eq (10) or (11) for a maximum of 1001 crystals, the new CSD is calculated, a new critical radius (r*) is determined, and ripening proceeds to the next calculation cycle. Because ripening occurs in a closed system, mass must be conserved. Therefore, during each calculation cycle the increase in volume of the crystals with radii greater than that of the critical radius is adjusted proportionately by the method discussed previously for open system

growth by supply-control (eq 8). This normalization matches the volume needed for growth with the mass made available for growth from dissolution of crystals having radii less than that of the critical radius. As ripening progresses, the mean diameter continues to increase, but the reaction slows until growth is barely perceptible. Therefore, the program realistically simulates this aspect of the natural process.

Mass balance requires that there are progressively fewer crystals in the system as the mean size increases. Since the program is limited to an initial maximum of 1001 crystals, large increases in mean size by ripening will lead to small numbers of crystals, and therefore to inaccurately determined shapes for CSDs. Good counting statistics are maintained, however, by iterating the ripening calculation, starting with the open system. Frequencies for the ripened CSDs for each iteration are added, and then divided by the number of iterations at the end of the calculation to find the final distribution.

Plots of progressive Ostwald ripening by supply-controlled kinetics of a lognormal CSD formed in the open system with a mean diameter of 7.7 nm (fig. 8A, and the dashed curves in fig. 8B, C, and D) lead to a shift in the CSDs (solid circles) to the right of the

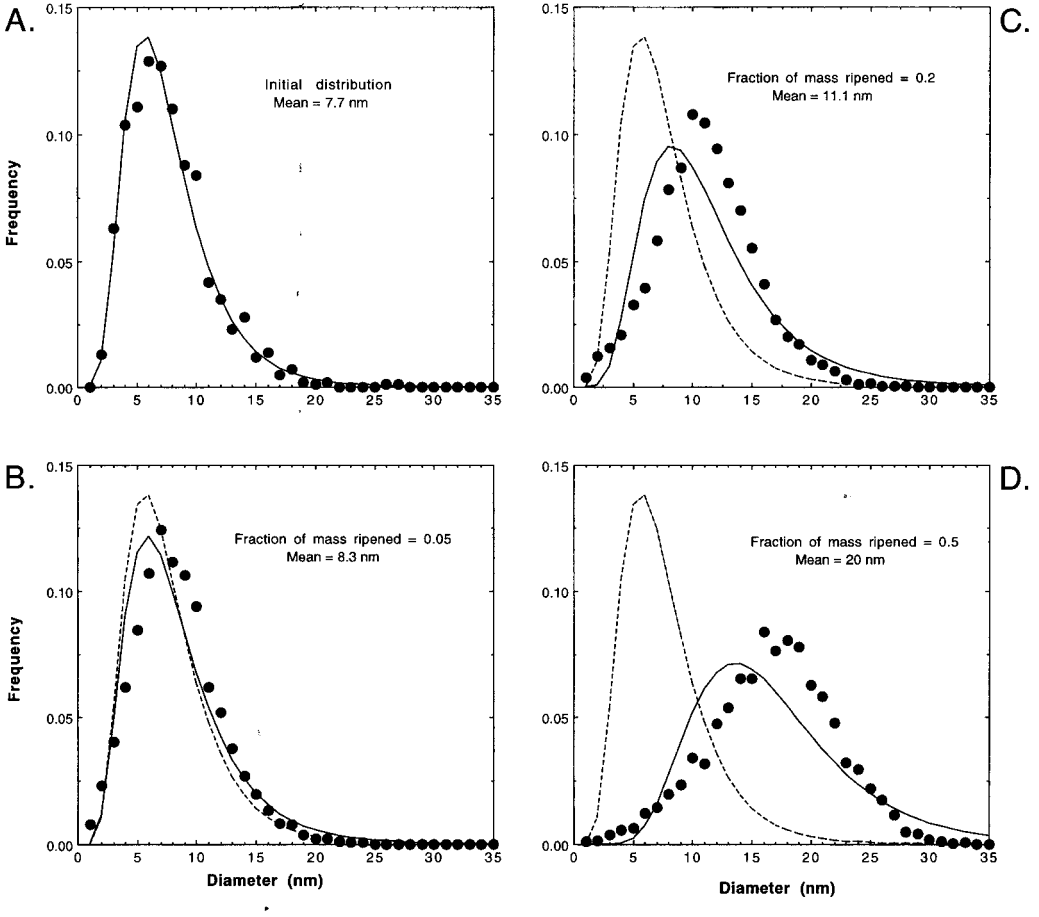

Fig. 8. GALOPER-calculated CSDs modified by Ostwald ripening. (A) = initial distribution; (B) = 5 percent of the initial mass has passed through solution once; (C) = 20 percent through solution; (D) = 50 percent through solution. The solid curves are theoretical lognormal curves calculated from the ripened CSDs (solid circles). The dashed curves are the shape of the original lognormal CSD in (A).

theoretical lognormal curves (solid lines in fig. 8B, C, and D), while the shapes of the CSDs become more symmetrical (fig. 8B and C), and finally skew in the opposite direction from the lognormal curves (fig. 8D). Ripening of initial CSDs having the asymptotic shape leads to a similar behavior.

The ripened CSDs in figure 8 are tending toward the shape of a universal function for supply-controlled ripening (eq A20 in app. 2). The end result of this process is a steady-state reduced plot given as a solid curve in figure 9A. The shapes of CSDs will tend toward this shape during supply-controlled ripening but may not reach it. For example, the lognormally-shaped CSD in figure 8A was ripened in GALOPER so that 90 percent of its mass passed through solution. The results in figure 9A (open circles) indicate that the steady-state shape is being approached by the calculation but has not been achieved. Similar plots are given in figure 9B for surface-controlled ripening. In figure 9B, the universal theoretical curve (solid line) was calculated from eq (A21) in app. 2, and 90 percent of the original mass of the initially lognormal CSD passed through solution (circles). If the ripening starts with a CSD having the universal steady-state shape, then theory predicts that this shape is maintained.

LSW theory also predicts that the mean diameter will vary linearly with the cube root of time for supply-controlled ripening (eq A15, app. 2) and with the square root of time for surface-controlled ripening (eq A19). Such plots are given in figure 10A and B, respectively, for several different rate constants, except that the data are plotted in terms of calculation cycles for eq (10) or eq (11), rather than in terms of time. The results are indeed linear and show that calculation cycles in the GALOPER program are analogous to time in the LSW theory.

Random ripening (supply-controlled).–During random ripening, crystals dissolve or grow randomly with respect to size because something other than specific surface area controls crystal solubility (for example, strain or environmental heterogeneity). In the GALOPER program, a random number between 0 and 1 is assigned to each of the 1001 crystals, and a probability for dissolution is entered. All crystals with a random number less than this probability dissolve completely during a series of cycles according to an equation similar to the LPE (eq 5, where the $\epsilon_j X_j$ terms have negative values) and supply nutrients to crystals that grow during the same series of cycles according to the LPE. During supply-controlled random ripening, dissolution during each calculation cycle proceeds at a rate slow enough to insure that the dissolved material is less than that required for growth by the LPE. Mass balance is maintained as discussed previously (eq 8).

The effects of supply-controlled random ripening are depicted in figure 11. An initial lognormal CSD having a mean diameter of 7.7 nm and a β^2 of 0.20 (fig. 11A) is ripened randomly so that 50 percent of its mass has passed through solution. The resulting lognormal CSD has a mean diameter of 9.5 nm and a β^2 of 0.21 (fig. 11B). The contrast between random ripening and Ostwald ripening is striking: (1) whereas during Ostwald ripening the shape of the CSD is modified (fig. 8), during random ripening the shape is maintained (fig. 11). As with supply-controlled open system growth, random ripening leads to steady-state shapes when CSDs are plotted on reduced axes, and (2) much more material must pass through solution for a given change in mean diameter during random ripening than during Ostwald ripening. For example, if 50 percent of the mass of a sample having an initial mean diameter of 7.7 nm passes through solution during the ripening process, the mean diameter increases to 9.5 nm for random ripening (fig. 11B) while increasing to 20 nm for Ostwald ripening (fig. 8D).

Other types of random ripening can be imagined. For example, a crystal could partially dissolve during one calculation cycle and grow during another. In this case, much material could pass through solution, but it would leave little record of this reaction in the shape of the CSD. One also could imagine surface-controlled random ripening during which β^2 would increase with the mean.

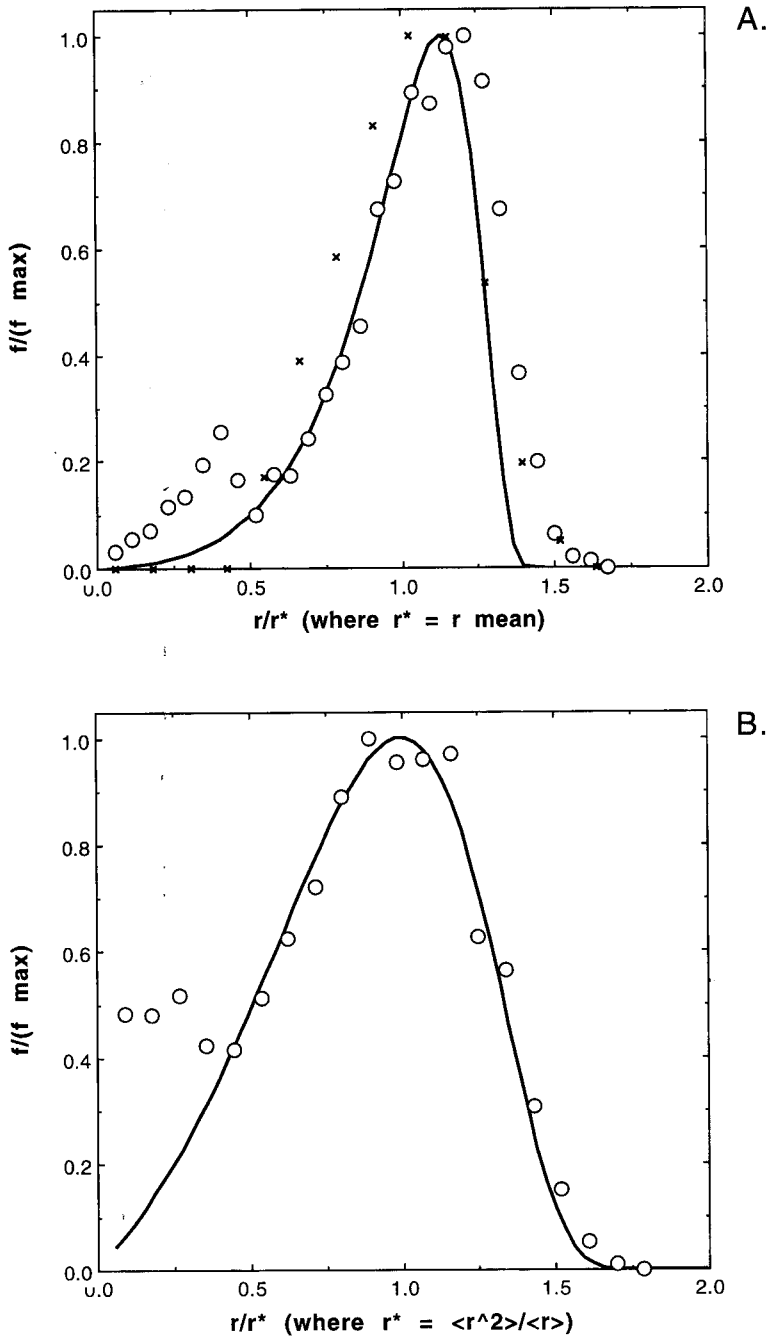

Fig. 9. Reduced plots for Ostwald ripening. (A) Universal reduced plot for supply-controlled Ostwald ripening (solid curve, calculated from eq A20) and a GALOPER-simulated ripening in which 90 percent of the material from an initially lognormal CSD passed through solution (circles). The x's are for garnet sample PM from Carlson and others (1995); (B) Universal reduced plot for surface-controlled Ostwald ripening (solid curve, calculated from eq A21) and a GALOPER-simulated ripening in which 90 percent of the material passed through solution (circles).

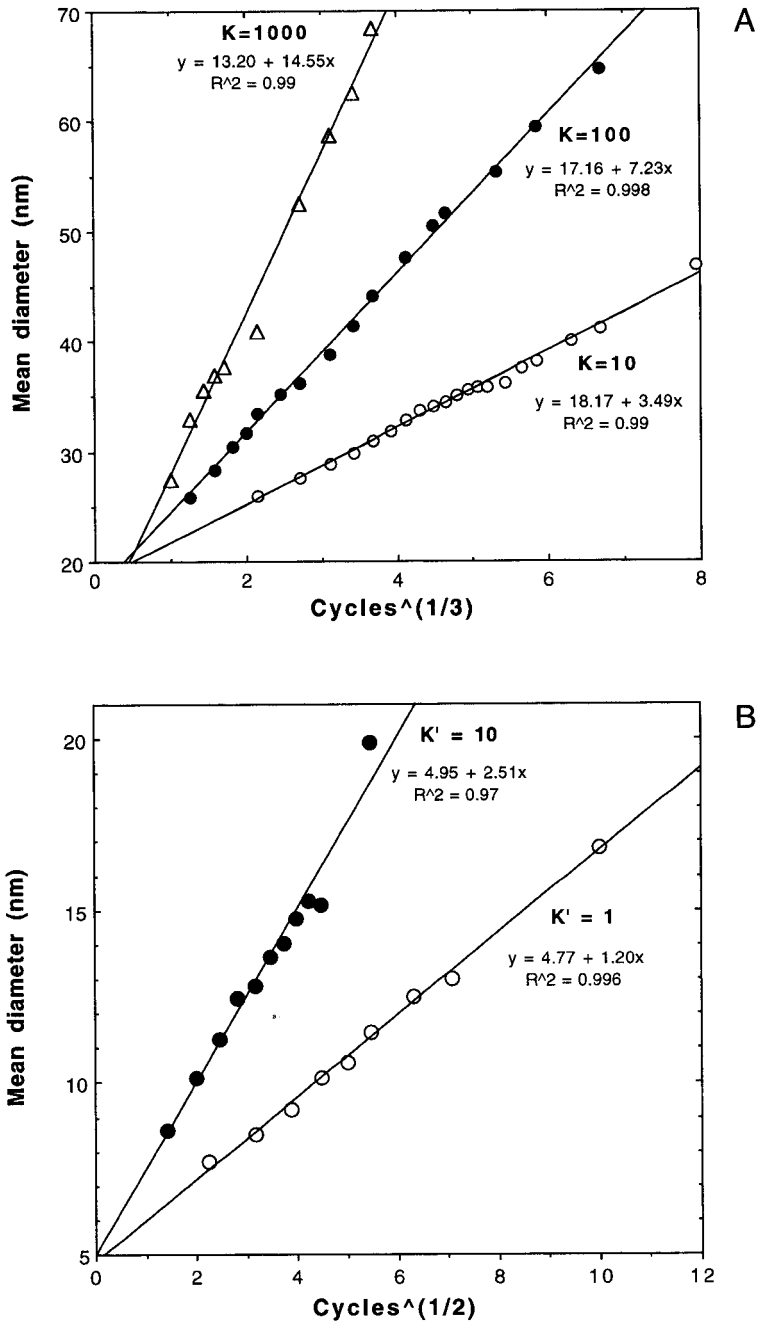

Fig. 10. Relation between number of cycles (time) and mean diameter for: (A) supply-controlled Ostwald ripening; and (B) surface-controlled Ostwald ripening.

Crystal agglomeration.–During growth by crystal agglomeration, two or more crystals grow together to become one large crystal. In the GALOPER program, a probability for crystal agglomeration is entered into the program, and a random number is assigned to each of the crystals during each calculation cycle. If a crystal's random number is less

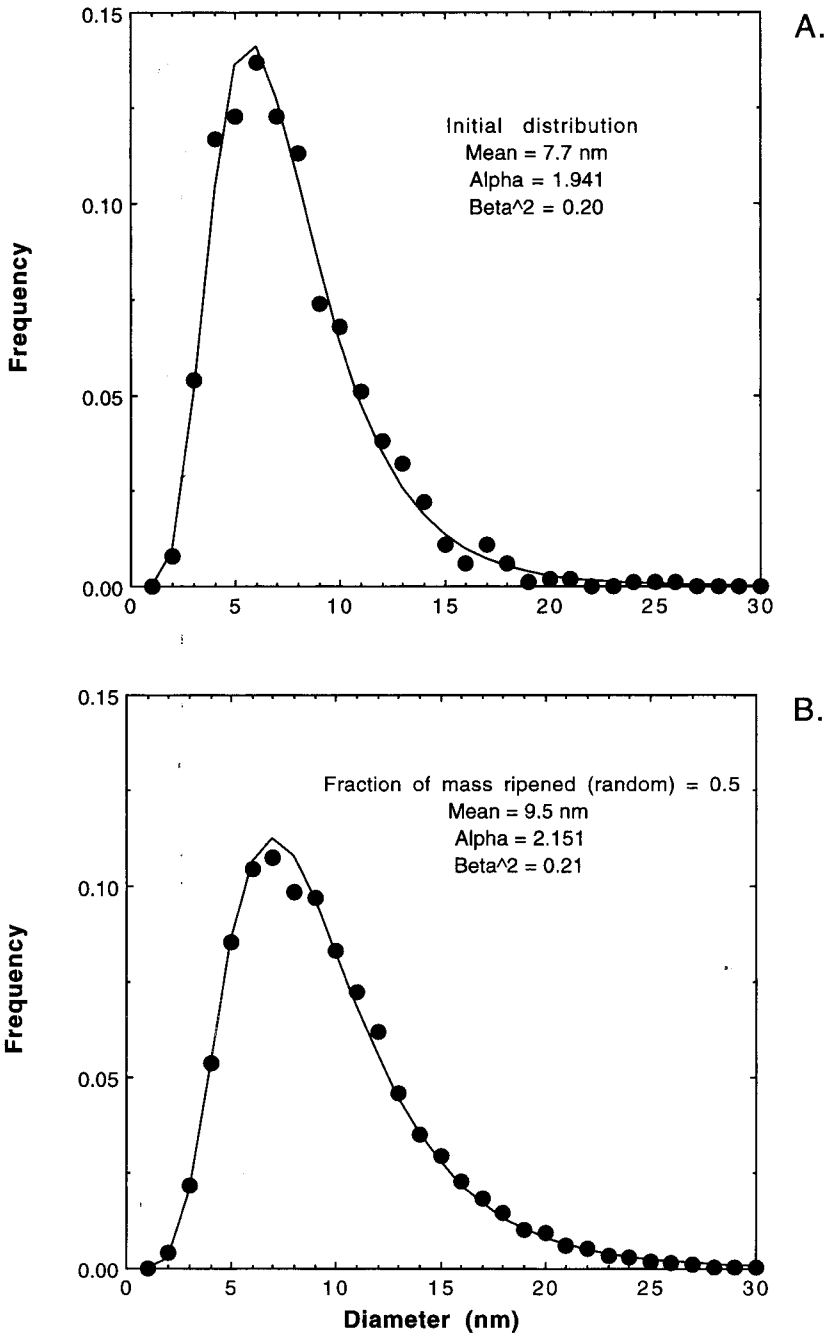

Fig. 11. GALOPER-calculated CSDs for random ripening. (A) = initial distribution; (B) = 50 percent of initial mass has passed through solution by supply-controlled random ripening. The solid circles are the calculated CSDs, and the solid lines are the theoretical lognormal curves.

than the entered probability, the crystal's size is added to that of the crystal below it on the spreadsheet, and the original crystal is removed from the system. Various rules may be applied concerning the size of crystals that are allowed to fuse together. Agglomeration may occur simultaneously with ripening, may be imperceptible, or may lead to multi-modal distributions.

SUMMARY OF RELATIONS BETWEEN CRYSTAL GROWTH MECHANISM AND CSD SHAPE

Crystal growth mechanisms and their effects on CSD shapes are summarized in table 2. Often it is possible to identify growth mechanisms from the shapes of individual CSDs, as is indicated in the table, but, in addition to considering the entire shape of the CSD, confidence is gained by determining the evolution of β^2 with respect to α for a series of related samples (fig. 12). Paths for surface-controlled growth in open systems (labeled 1-3 in the figure) are linear, change slope with changes in system variability (ϵ), and change intercept with changes in initial crystal size. For example, curves 1 and 2,

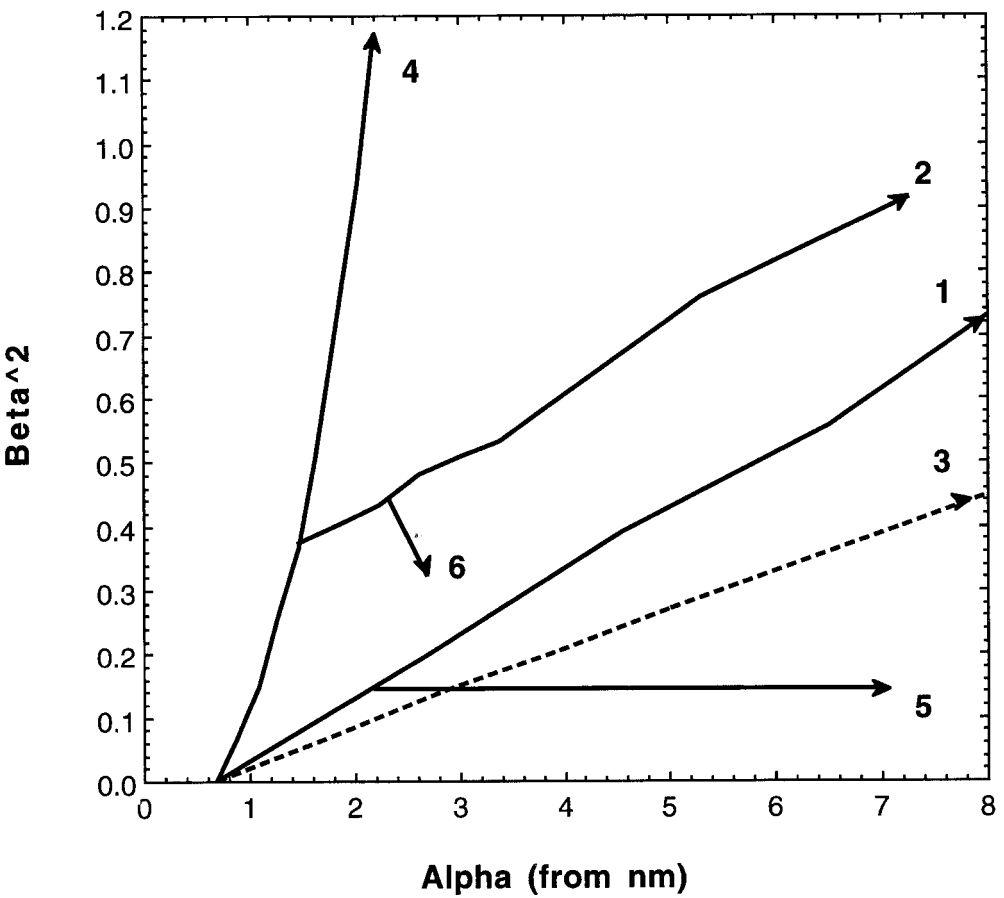

Fig. 12. Theoretical paths through a α-β^2 space for growing crystal size distributions, calculated using GALOPER. 1 and 2 = paths for surface-controlled open system growth assuming starting crystal diameters of all 2.0 and an asymptotic distribution have a mean size of 5.2 nm, respectively; 3 = path for the same calculation as curve 1, but letting ϵ vary from 0 to 0.5 rather than between 0 and 1; 4 = path for continuous nucleation and growth, with a critical nucleus of 2 nm; 5 = generalized path for supply-controlled open system growth or random ripening; 6 = generalized path for Ostwald ripening.

which have the same slope but different intercepts, indicate parameter evolution for systems in which ϵ varies between 0 and 1. However, curve 1 began with an initial distribution containing only 2.0 nm crystals, whereas curve 2 started with an asymptotic distribution, having a mean size of 5.2 nm, that was formed by continuous nucleation and growth, and that was then modified by surface-controlled growth. Curve 3, like curve 1, started with and initial crystal size of 2 nm and therefore has the same intercept as curve 1, but system variability (ϵ) was allowed to vary between 0 and 0.5, rather than between 0 and 1, and therefore it has a smaller slope. A smaller system variability could represent, for example, a better stirred system if variability is related to solution heterogeneities. In all other calculations except that for curve 3, ϵ was allowed to vary only between 0 and 1.

During continuous nucleation and growth with a constant nucleation rate, β^2 increases exponentially with α. For example, curve 4 in figure 12 represents continuous nucleation and growth using a critical nucleus size of 2.0 nm. Path 5 is arbitrarily chosen (that is, not calculated) to represent supply-controlled growth or random ripening, during which β^2 remains constant as the mean increases. Finally, an arbitrarily chosen path 6 for Ostwald ripening indicates that β^2 decreases with increasing mean size. Ostwald ripening is the only mechanism by which variance decreases as mean size increases, except for certain types of agglomeration in which most of the crystals are involved.

DISCUSSION AND EXAMPLES

Examples of continuous nucleation and growth.–Figure 13 gives examples of measured CSDs that have asymptotic-type shapes, which the GALOPER calculations suggest were formed by the constant-rate nucleation mechanism. The phlogopite sample (fig. 13A) was formed from a gel after 10 min at 600°C and 1 kb in an experimental hydrothermal system (Baronnet, 1974). The Le Puy illite (fig. 13B) formed in a saline, alkaline lake in the Massif Central, France (Gabis, 1963). The magnetite (fig. 13C) is from hornfels facies rock from Skye (Cashman and Ferry, 1988). The AgBr crystals (fig. 13D) were precipitated by running a solution of 200 g of silver nitrate in 1 L of water into a bromide-gelatin solution containing 1700 g of water. The addition of silver nitrate was adjusted to last for 10 min and was constant (Loveland and Trivelli, 1947).

The nucleation (constant rate) and surface-controlled growth mechanism was used to simulate the phlogopite (fig. 13A) and the illite (fig. 13B) CSDs. The calculations were carried out by matching the calculated mean sizes with those of the samples, using a critical nucleus size of 2.0 nm. A better match between experiment and simulation was found for the phlogopite, if continuous nucleation and growth was followed by some open system growth without nucleation. The results from GALOPER simulations for both CSDs appear to match the data (fig. 13); however, Chi-square analysis gives a significance level <1 percent (table 1).

Parameters for CSDs shown in figure 13 are plotted in figure 14. The uppermost point for phlogopite, which is the synthetic, 10 min, hydrothermal sample, plots slightly to the right of the continuous nucleation and growth trend, indicating that growth by this mechanism may have been followed by some surface-controlled growth, as also was indicated above by GALOPER simulation of the CSD shape. The left-most trend for illites, which includes the Le Puy illite, follows that expected for continuous nucleation and growth. The curves for the AgBr and magnetite samples have the correct slope for continuous nucleation and growth but plot to the right of the theoretical trend, indicating that growth by this mechanism may have been followed by supply-controlled growth or by random ripening, which would increase size without changing variance.

Examples of surface-controlled open system growth.–Thickness distributions (fig. 15) for fundamental illite crystals (that is, the smallest physically separable illite platelets; see Nadeau and others, 1984) are readily simulated using the open system, surface-

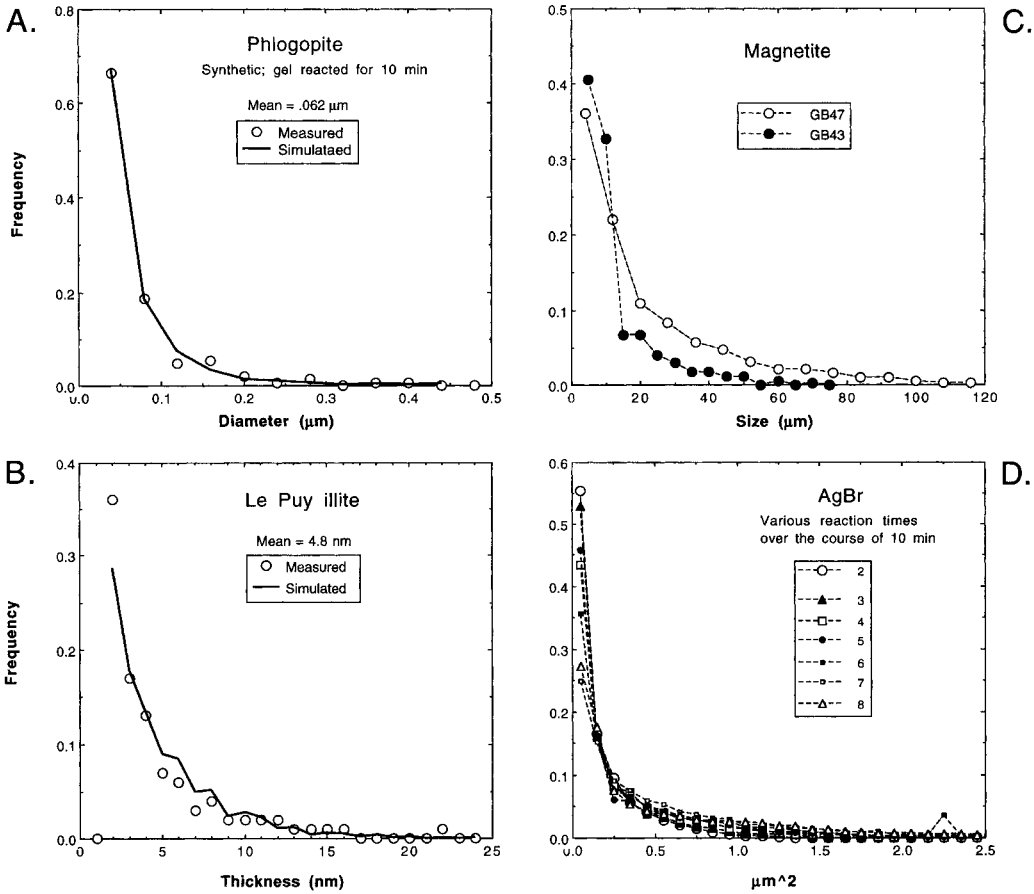

Fig. 13. Measured asymptotic-type CSDs for minerals, and GALOPER simulations. Shapes of CSDs are attributed to nucleation and growth with constant nucleation rate. (A) Phlogopite mean a-b diameters from Baronnet (1974 and personal communication), with GALOPER simulation (solid curve); (B) Le Puy illite thickness distribution, measured by the Bertaut-Warren-Averbach XRD method (Drits and others, 1998; Eberl and others, 1998), and GALOPER simulation (solid curve); (C) Magnetite from Cashman and Ferry (1988); AgBr data from Loveland and Trivelli (1947; L-1 precipitation, their fig. 7).

controlled growth mechanism (Środoń and others, submitted). It has only proved necessary to match the calculated mean thicknesses to the measured mean thicknesses. The simulation for the Zempleni illite started with an initial crystal thickness of 1 nm, and the others started with 2 nm. All but one of the Chi-square tests demonstrate matches at the >20 percent significance level between the measured distribution and the theoretical lognormal curves and between the measured distribution and the GALOPER simulations (table 1). The significance level for the exception (RM35A illite and the GALOPER simulation) is at the 5 to 10 percent level. The trends in lognormal parameters for illite fundamental particle thickness distributions for a series of hydrothermal and diagenetic illite samples collected from a variety of locations (right illite trend in fig. 14) also indicate surface-controlled, open system growth.

Examples of supply-controlled open system growth.—The only known growth mechanism that evolves toward a lognormally-shaped CSD is surface-controlled growth (LPE growth). Therefore, all the minerals depicted in figure 1, with the possible exception of

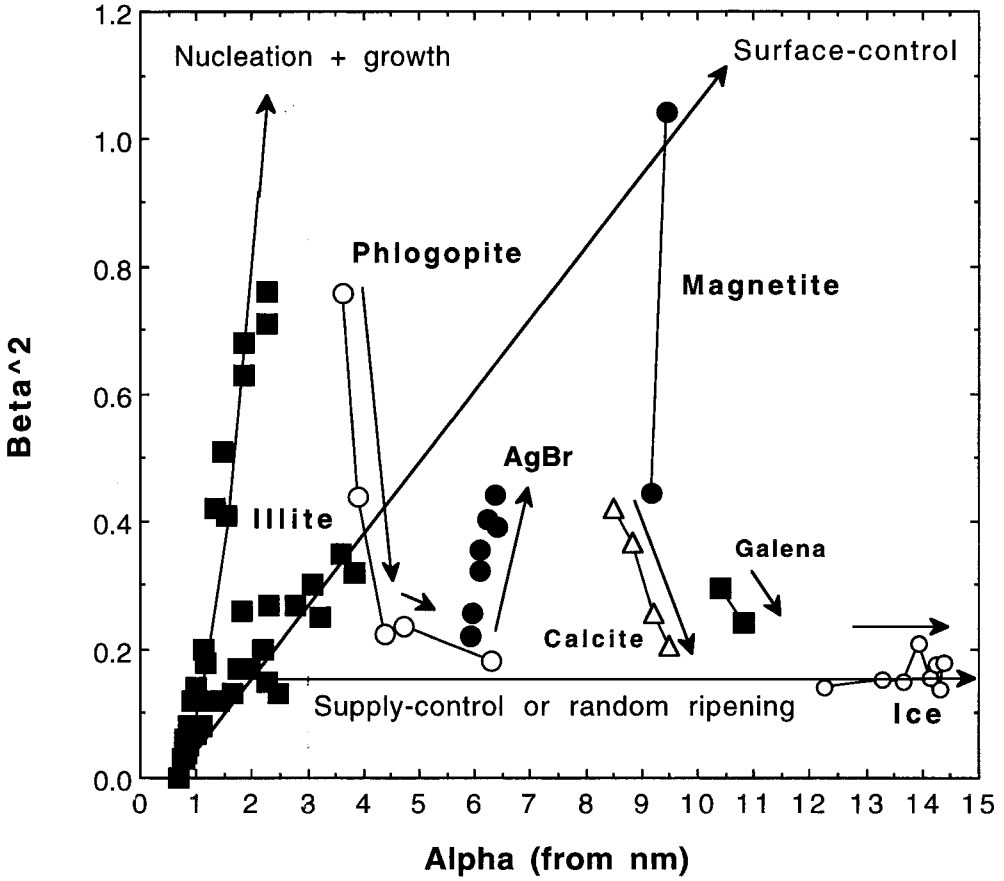

Fig. 14. Diagram as in figure 12 on which have been plotted measured variations in α-β^2 for CSDs of natural and synthetic minerals. AgBr from Loveland and Trivelli (1947; see fig. 13D; μm^2 reported were converted into diameters); phlogopite from Baronnet (1974 and personal communication; see fig. 13A); calcites from Chai (ms; see fig. 18); Galena from Stanton and Gorman (1968); Ice from Colbeck (1986 and personal communication; see fig. 1F); Magnetites from a basaltic hornfels from Skye (Cashman and Ferry, 1988; see fig. 13C). Illites (see figs. 13B and 15) from Eberl and others (1998) and Środoń and others (submitted) for area-weighted, illite fundamental particle thickness distributions (smectite monolayers are excluded from the data).

the sphene sample, must have experienced this mechanism at some time during their growth history. However, if crystals grew only by this mechanism, then the CSDs should be very broad at large mean sizes, because β^2 increases linearly with mean size (fig. 12). For example, garnet 711A (fig. 1A, with $\alpha = 13.08$ and $\beta^2 = 0.14$) plots far to the right of the curves that yield lognormal CSDs (curves 1-2 in fig. 12). The lognormal shape of this garnet's CSD is best explained by two growth stages: (1) an early stage during which the lognormal profile was established (for example, the initial part of curve 1, fig. 12), and (2) a later stage of supply-controlled open system growth or random ripening (curve 5, fig. 12) when the crystals grew larger while preserving β^2 from the previous stage. Many minerals probably follow a crystallization path similar to that depicted for the garnet, because the amount of nutrients required to maintain nucleation and surface-controlled growth in the open system increases exponentially with mean crystal size. In response to this exponentially increasing requirement for mass, minerals in general may leave the

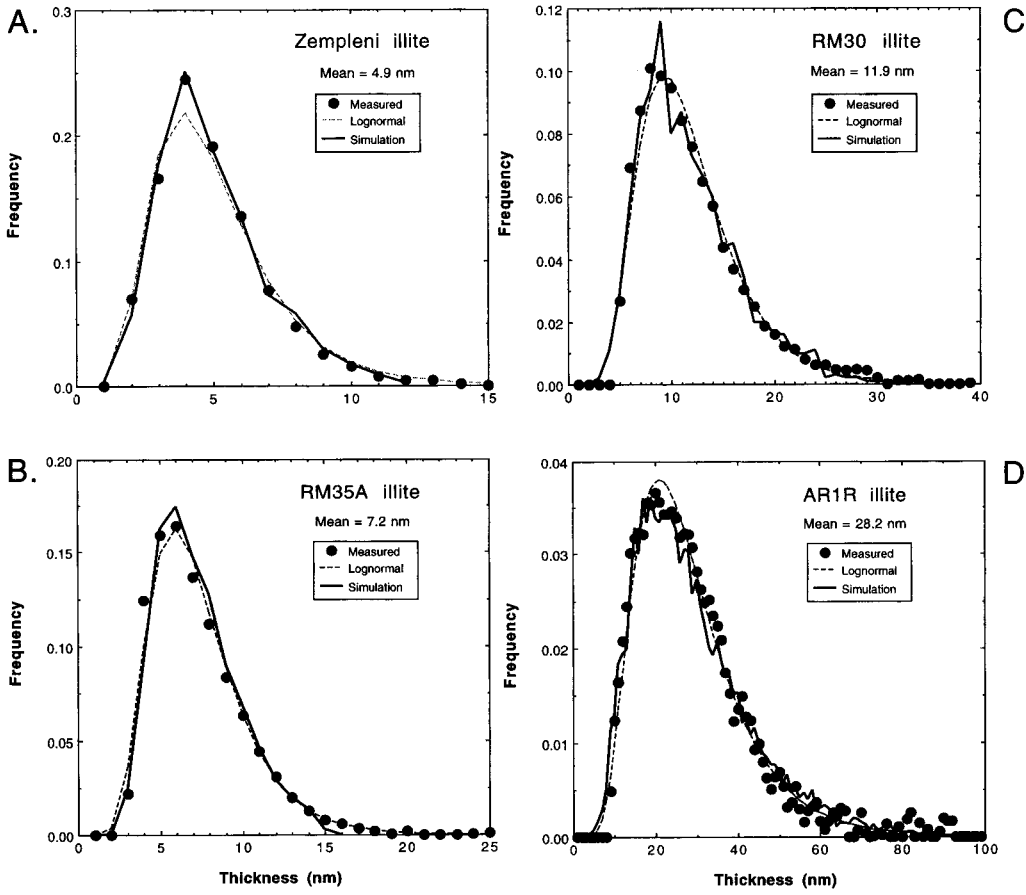

Fig. 15. Fundamental illite crystal thickness distributions for hydrothermal illites, measured by the authors by X-ray diffraction (Drits and others, 1998; Eberl and others, 1998). Points = measured distributions; dashed lines = lognormal curves calculated from the measurements; solid lines = GALOPER simulations. For information on the samples: (A) (Viczián, 1997); (B, C, and D) (Eberl and others, 1987).

path of surface-controlled growth at about the same mean size to begin supply-controlled growth (path 5 in fig. 12). Thus, their β^2's should be approximately equal no matter what their final size. Therefore, their CSDs should follow steady-state reduced plots, as is demonstrated in figure 16 for diverse minerals depicted in figure 1.

Another possible example of supply-controlled growth in an open system may be found in a peritidal environment in Belize (Gregg and others, 1992) in which dolomite crystals have lognormal CSDs (table 1). The mean size increases with depth (fig. 17), from 0.42 μm near the top of the profile to 0.91 μm at 30.2 cm depth. Except for the uppermost sample, β^2 remains approximately constant at about 0.13 throughout. The CSDs in this profile could not have developed solely from open system surface-controlled growth, because β^2 has not increased with mean size. A significant amount of Ostwald ripening also can be ruled out because the CSD would have moved to the right of the theoretical lognormal curves (see fig. 8). Also, the crystals may be too large to have sufficient differences in specific surface free energy at such a low temperature to drive the Ostwald ripening process. Morse and Wang (1995) indicate that ripening would be effective at sizes below 0.1 μm in such systems. The profiles could result from random

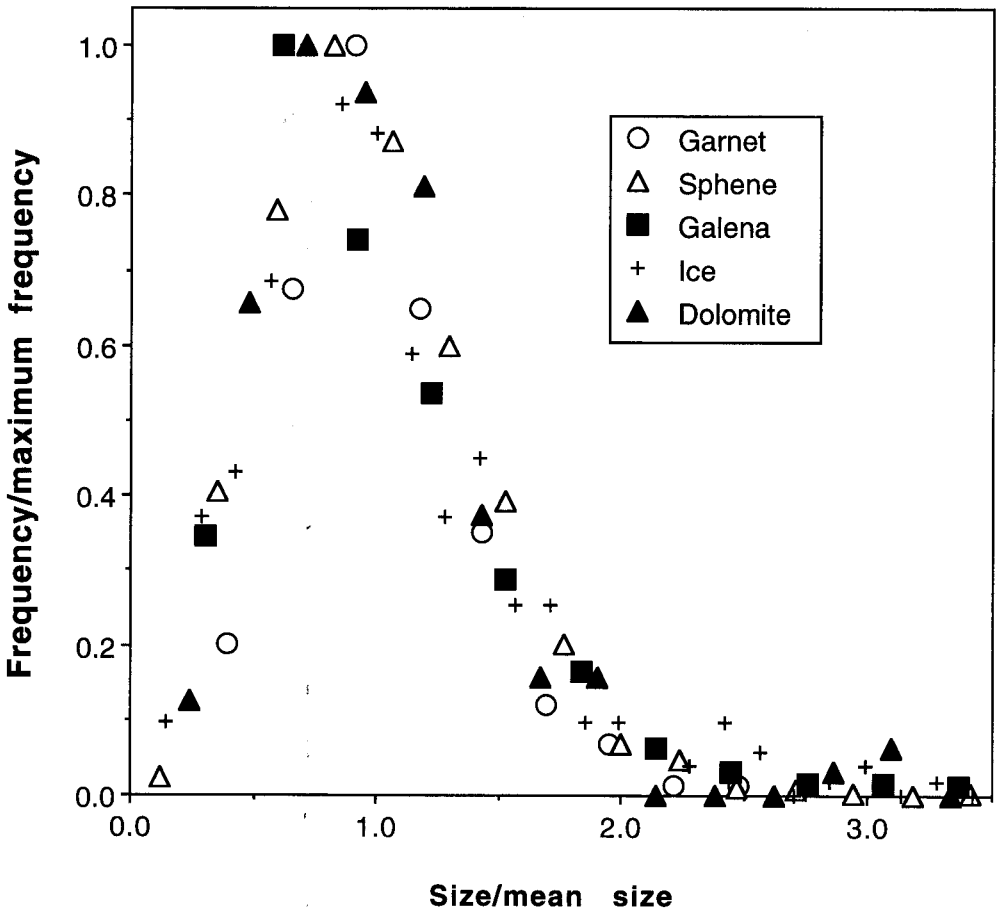

Fig. 16. Reduced CSDs calculated for minerals in figure 1, demonstrating steady-state shape.

ripening, if the system were closed to nutrient influx, which seems unlikely for this type of environment. The three deepest samples (fig. 17) seem to display a circumflex, a feature discussed previously, that may have been inherited from an asymptotic-type distribution formed during the nucleation stage.

Evidence for supply-controlled growth also comes from CSDs for garnets (sample PM in Carlson and others, 1995; and several distributions in Miyazaki, 1991) which approximate the universal steady state distribution (fig. 9A) expected for supply-controlled Ostwald ripening. However, mean crystal sizes for these samples are measured in millimeters, and their crystal size distributions are narrow. Therefore differences in specific surface free energy between small and large crystals are negligible (Morse and Wang, 1996) and can not drive an Ostwald ripening process. The Ostwald profile must have developed early in the garnets' growth histories, when the crystals were much smaller, and the shape of the CSD then was preserved as the crystals grew larger by supply-controlled growth or by random ripening.

Examples of ripening.–Perhaps the most comprehensive study of ripening is that of Chai (1973; ms), and Anderson and Chai (1973) for calcite recrystallized in hydrothermal bomb experiments. One series of experiments (table 5 in Chai, ms) used Fisher

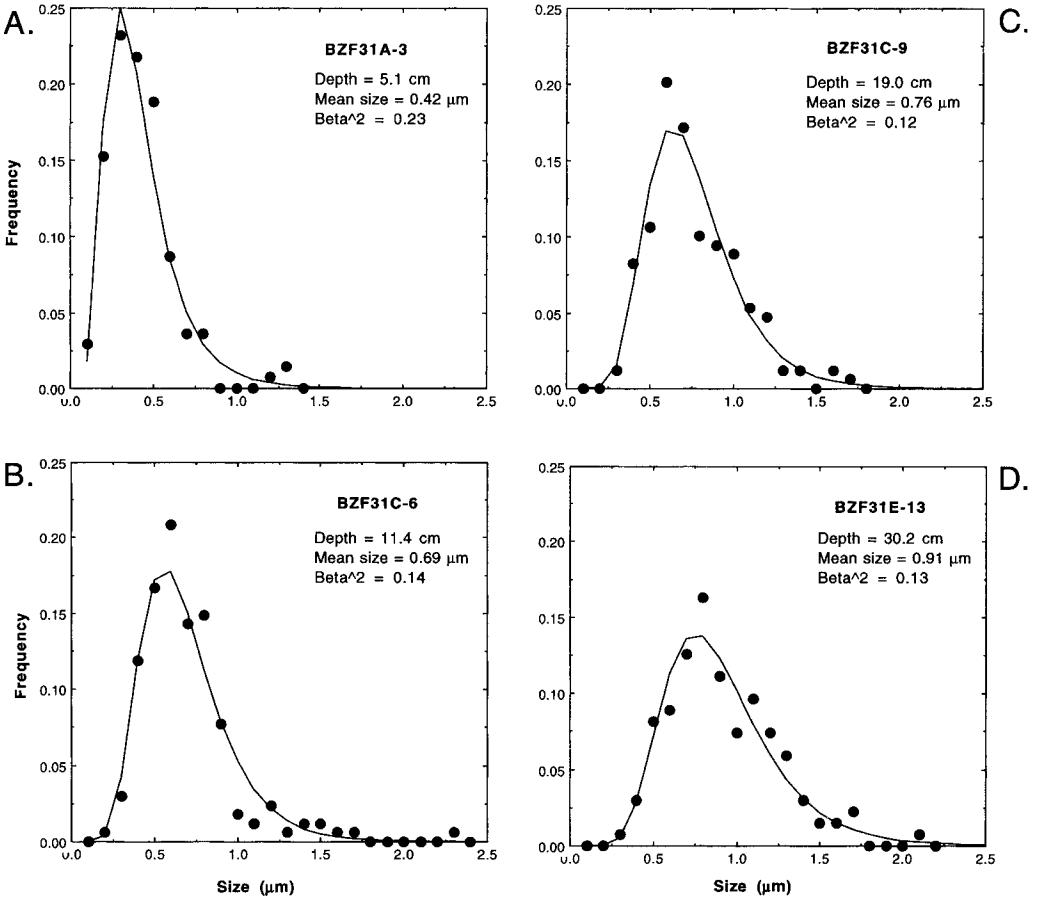

Fig. 17. Measured CSDs (symbols) compared with theoretical lognormal curves (solid lines) for dolomite CSDs collected at various depths from crusts from the bottom of Ambergris Cay, Belize (Gregg and others, 1992, and personal communication).

calcite as the starting material. It was reacted at 500°C and 2 kb pressure for different lengths of time, and the fraction of material that passed through solution was calculated from changes in calcite oxygen isotopes.

Figure 18 gives the particle size distributions (solid circles) measured by Chai for the starting material (fig. 18A) and for calcites that reacted for three different lengths of time (fig. 18B, C, and D). The figure also shows theoretical lognormal distributions calculated from Chai's measurements (dashed curves) and the GALOPER simulations (solid curves). The latter were calculated by ripening the original lognormal (table 1) Fisher calcite distribution to the mean sizes of the measured CSDs by the mechanisms of random and Ostwald ripening, as will be discussed below, in the proportions predicted from figure 19. During ripening, the measured CSDs move to the right of the theoretical lognormal distributions, as is predicted by theory (fig. 8), and are matched by the GALOPER simulated CSDs (table 1).

The fraction of calcite recrystallized, as measured by isotopic analysis, is plotted as a function of mean crystal diameter in figure 19 (solid circles), with increasing mean size corresponding to increasing reaction time. The GALOPER simulation for Ostwald

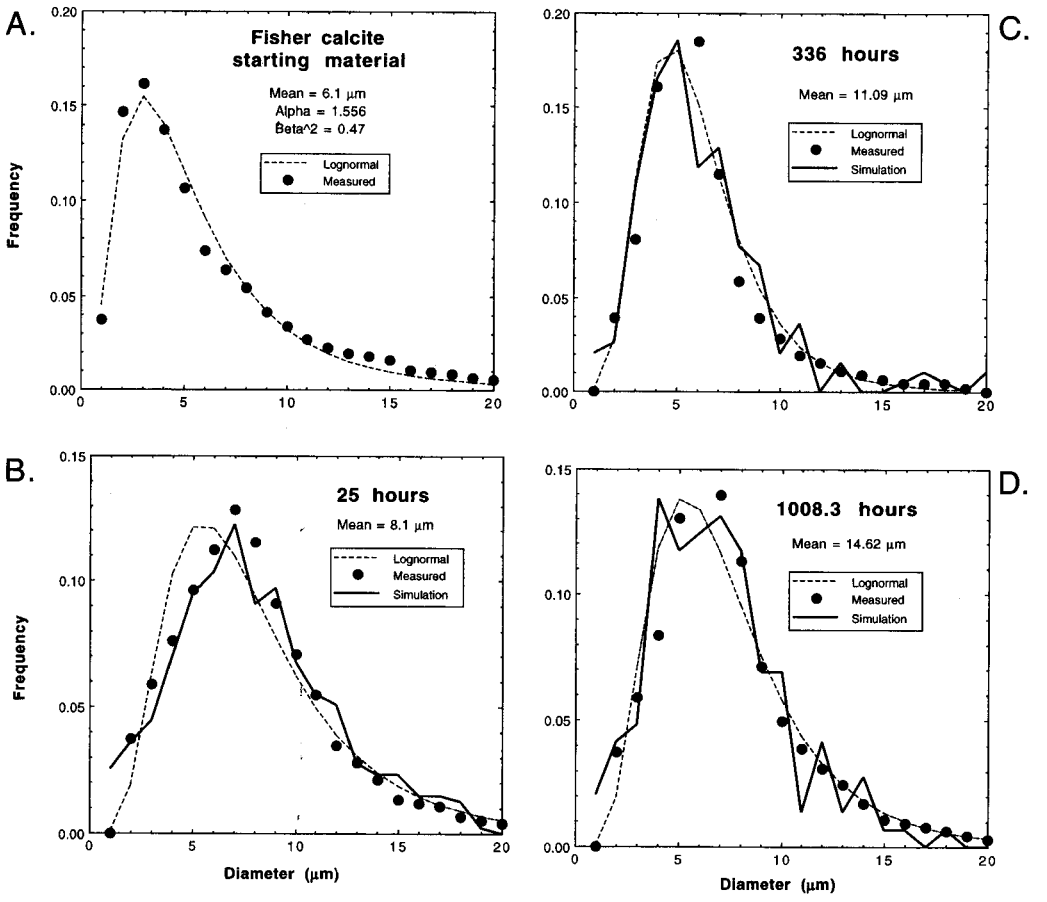

Fig. 18. CSDs (from figs. 44 and 45 in Chai, ms) from calcite ripening experiments compared with theoretical lognormal (dashed curves) and GALOPER simulations (solid curves). The initial Fisher calcite was ripened at 500°C and 2 kb for different lengths of time.

ripening (lower line in fig. 19) does not fit these data. The simulation predicts a much smaller amount of recrystallization for a given increase in mean crystal diameter. If the simulation is correct, then a process other than Ostwald ripening must have occurred in the experiments. It seems unlikely that the Fisher calcite, initially formed at low temperatures, would react completely by surface-area driven recrystallization when taken to 500°C. The crystals may contain defects, sharp edges, other imperfections, and other polymorphs that may destabilize crystals of all sizes when exposed to an environment radically different from that of its initial, low temperature formation.

The upper curve in figure 19 is a GALOPER calculation for purely random ripening. The measurements fall between the two calculated endmember mechanisms and indicate that the calcites may have reacted by both mechanisms, with random ripening accounting for approx 80 to 85 percent of the material that passed through solution. Thus, the shapes of the calcite CSDs are a function of Ostwald ripening, whereas the major fraction of material passing through solution is a function of random ripening.

Pathways in α-β^2 space for several experimental Ostwald ripenings are indicated by descending arrows in figure 14. β^2 decreases as ripening proceeds, and the CSDs (not

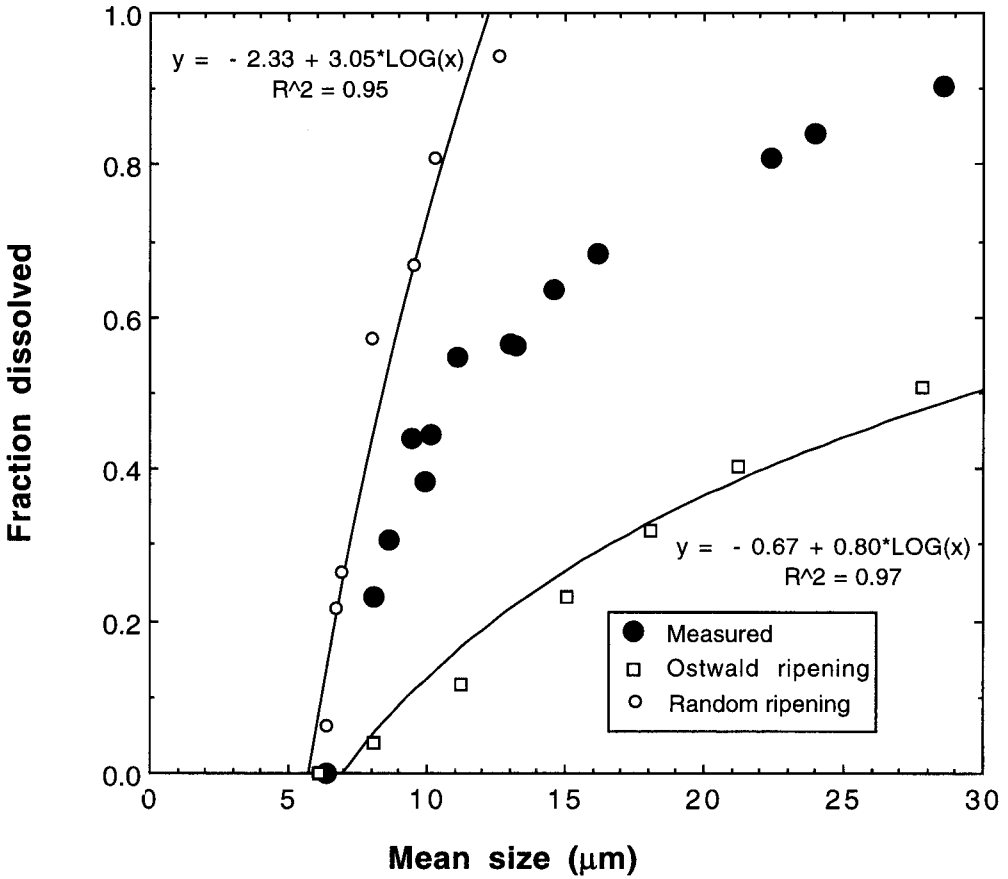

Fig. 19. Fraction dissolved (from oxygen isotope measurements) versus increase in mean crystal size for calcite ripening experiments, compared with theoretical, GALOPER-calculated curves for random ripening (upper curve) and Ostwald ripening (lower curve). Data from table 5 in Chai, ms).

shown) have the characteristic, more symmetrical shapes that lie to the right of theoretical lognormal curves. The exception is the shapes of CSDs for ice crystals ripened in a water-saturated system (Colbeck, 1986, 1987). In this system, the rate of crystal growth is a function of the rate of heat transfer, rather than the rate of mass transfer. These CSDs retained their lognormal shapes during ripening, and β^2 remained constant (fig. 14), suggesting that random ripening may have played a role in this process.

CONCLUSION

In systems that are very close to equilibrium, conventional kinetic and thermodynamic theories are useful, and the equations for Ostwald ripening indicate that reaction rates are proportional to differences in diffusion rate and to differences in surface free energy, as is expected from the principle of detailed balancing (Lasaga, 1981). Assuming that crystals of the same phase have identical internal and surface energies, Ostwald ripening rates are proportional to differences in specific surface area (area/volume, or 1/r in eqs 10 and 11).

Systems that are far from equilibrium may be very heterogeneous; therefore, conventional thermodynamic and kinetic theories are difficult to apply. The Law of

Proportionate Effect, chosen because it yields correct lognormal shapes for CSDs for many minerals, and because it describes size dependent growth and growth dispersion, has proven to be a simple approach for modeling the complex phenomena of crystal growth in such systems. This law (eq 5) indicates that crystals will tend to grow in proportion to their size. It is remarkable that such an apparently vague prediction can lead to such exact results for simulating the growth of crystal size distributions.

The present approach recognizes three basic shapes for CSDs: lognormal, asymptotic, and a universal steady state shape. These shapes identify three mechanisms for crystal growth: surface-controlled growth, continuous nucleation and growth, and Ostwald ripening, respectively. Intermediate shapes also are possible as one CSD shape is transformed into another by a change in growth mechanism. In addition, there are two growth mechanisms that are hidden because they adopt the shape of the previous CSD: supply-controlled growth and random ripening. Crystals may undergo a sequential change in growth mechanisms as environmental conditions (especially levels of supersaturation) change during crystal growth. Changes in growth mechanism not only affect the shape of the CSD but also the rate law for crystal growth.

ACKNOWLEDGMENTS

The authors thank A. Baronnet, S. Colbeck, and J. Gregg for furnishing original particle size analysis data, and A. Blum, H. May, J. Neil and M. Davis for reviewing the original manuscript. J. Środoń and V. Drits thank the U.S. Geological Survey and V. Drits thanks the Russian Science Foundation for vital financial support during this research.

Appendix 1

The law of proportionate effect

The derivation below generally follows that of Koch (1966). The Law of Proportionate Effect is:

$$X_{j+1} = X_j + \epsilon_j X_j, \tag{A1}$$

where X_j is some specified dimension in a crystal, ϵ_j is a small, randomly varied number, and X_{j+1} is the new crystal dimension after one growth cycle. If eq (A1) is iterated several times for many crystals, the final distribution can be shown to be lognormal.

According to the central limit theorem, a normal (bell-shaped or Gaussian) distribution can be generated by addition of small, independent, random variables to a quantity. A lognormal distribution can be generated similarly by adding the same type of variables to the logarithm of a quantity. Rewriting eq (A1):

$$X_{j+1} = X_j(1 + \epsilon_j),$$

and

$$X_1 = X_0(1 + \epsilon_1). \tag{A2}$$

For n number of calculation cycles, one can rewrite the above equation:

$$X_n = X_0 \prod_{j=1}^{n} (1 + \epsilon_j), \tag{A3}$$

where X_0 is the initial size, and Π is the product of $(1 + \epsilon_j)$ for the variable j. Taking the logarithms of both sides:

$$\ln X_n = \ln X_0 + \sum_{j=1}^{n} \ln(1 + \epsilon_j). \tag{A4}$$

The logarithm can be expanded for values of ϵ that are small compared to 1:

$$\ln(1 + \epsilon) = \epsilon - \frac{\epsilon^2}{2} + \frac{\epsilon^3}{3} - \frac{\epsilon^4}{4} \cdots. \tag{A5}$$

Because the terms raised to a power in the above equation are small, they can be ignored, and the result substituted into eq (A4) to yield:

$$\ln X_n = \ln X_0 + \sum_{j=1}^{n} \epsilon_j \tag{A6}$$

Therefore, according to the central limit theorem, the logarithms of the crystal sizes ($\ln X_n$) will be normally distributed.

A mean value for ϵ_n can be used to calculate the final mean size ($\overline{X}_n$) of a CSD from the initial mean size ($\overline{X}_0$). This calculation is possible because the variation in ϵ_n is identical within each cycle, and is independent from crystal size. In accordance with eq (A6):

$$\ln(\overline{X}_n/\overline{X}_0) = n\frac{\sum_{i=1}^{n}\epsilon_j}{n} = n\bar{\epsilon}, \text{ or } \overline{X}_n = \overline{X}_0 \exp(n\bar{\epsilon}). \tag{A7}$$

The proof that the LPE yields a lognormal distribution requires that the values of ϵ be small compared with one, but calculation shows that a good approximation to the lognormal distribution is realized even if ϵ is allowed to vary between 0 and 1. If ϵ_{max} is large and if ϵ varies between ϵ_{min} and ϵ_{max}, then eq (7A) should be replaced by a modified form of eq (A4):

$$\ln(\overline{X}_n/\overline{X}_0) = n\frac{\sum_{j=1}^{n}\ln(1+\epsilon_j)}{n} = n\ln\left(1 + \frac{(\epsilon_{max} + \epsilon_{min})}{2}\right),$$

then

$$\overline{X}_n = \overline{X}_0\left(1 + \frac{\epsilon_{max} + \epsilon_{min})}{2}\right)^n = \overline{X}_0(1 + \bar{\epsilon})^n. \tag{A8}$$

If $\bar{\epsilon} \ll 1$, then eq (A8) is transformed into eq (A7).

Appendix 2

Ostwald ripening

According to Wagner (1961) a growth (or dissolution) rate of crystals is expressed by the equation:

$$\frac{dr}{dt} = \frac{2\gamma C_0 \nu}{kT}\frac{D}{\eta r + D}\left(\frac{1}{r^*} - \frac{1}{r}\right), \tag{A9}$$

where r is the crystal radius, t is time (or calculation cycles), r^* is the critical radius of a crystal that is in equilibrium with solution, D is the solute diffusion coefficient, η is a parameter describing the rate-limiting process at the interface boundaries, γ is the interfacial free energy, ν is the atomic volume of the solute, C_0 is the concentration of the saturated solution, k is the Boltzman constant, and T is the absolute temperature.

Eq (A9) was obtained when the condition $dr/dt = 0$ was satisfied for a crystal having the critical radius:

$$r^* = \frac{\int f(r, t)\frac{r^2 dr}{\eta r + D}}{\int f(r, t)\frac{r dr}{\eta r + D}}, \tag{A10}$$

where f(r, t) describes the crystal size distribution as a function of time.

The condition $dr/dt = 0$ for crystals having the critical radius expresses the condition of equilibrium between crystals and solution. If $r > r^*$ the crystal grows; if $r < r^*$ it dissolves. An evolution of the crystal growth system with time, t, leads to an increase of r^* according to the equation (Wagner, 1961):

$$t = q_i\left(\frac{kT}{2\gamma C_0 \nu}\right)\frac{(r^{*2})(\eta r^* + D)}{\eta D}. \quad \text{(A11)}$$

q_i is a constant that depends on specified crystal growth conditions. Eqs (A9) and (A10) show that crystal growth rate, as well as critical radius values, are strongly controlled by a diffusion coefficient value; that is, they depend on the supply of available nutrients.

Let us consider two extreme cases which may correspond to diffusion-controlled ripening (D is small) or to surface-controlled ripening (D is large). In the first case, $\eta r \gg D$, and the instantaneous rate at which a given crystal grows (or dissolves) is obtained from eq (A9) by omitting D in the term $(\eta r + D)$:

$$\frac{dr}{dt} = \frac{2\gamma C_0 \nu D}{\eta kTr}\left(\frac{1}{r^*} - \frac{1}{r}\right). \quad \text{(A12)}$$

Replacement of $(\eta r + D)$ by ηr in eq (A10) shows that in the given case a critical radius is equal to the mean dimension of the crystals, $\bar{r}$, since:

$$r^* = \frac{\int f(r, t)rdr}{\int f(r, t)dr} = \bar{r}. \quad \text{(A13)}$$

A similar operation transforms eq (A11) and reveals a relation between r^* and time, t. Note that for diffusion-controlled conditions, $q_i = 9/4$ (Wagner, 1961). Thus

$$t = \frac{9kT(r^*)^3}{8\gamma C_0 \nu D}, \quad \text{(A14)}$$

and

$$r^* = \bar{r} = \left(\frac{8\gamma C_0 \nu D t}{9kT}\right)^{1/3}. \quad \text{(A15)}$$

Eq (A15) shows that at relatively large time, the crystal radius should asymptotically increase with time as $t^{1/3}$.

In the second case, $D \gg \eta r$ in eqs (A9) and (A10). This case corresponds to surface-controlled kinetics. The equations describing a crystal growth rate and a critical radius value can be obtained from eqs (A9) and (A10), respectively, omitting ηr in the term $(D + \eta r)$.

The corresponding equations are transformed:

$$\frac{dr}{dt} = \frac{2\gamma C_0 \nu}{kT}\left(\frac{1}{r^*} - \frac{1}{r}\right), \quad \text{(A16)}$$

and

$$r^* = \frac{\int r^2 f(r, t)dr}{\int rf(r, t)dr} = \frac{\overline{r^2}}{\bar{r}}. \quad \text{(A17)}$$

Replacement of $(D + \eta r)$ by D in eq A11 shows that the critical radius should asymptotically increase with time as $t^{1/2}$, since

$$t = 2\left(\frac{kT}{2\gamma C_0 \nu \eta}\right)(r^*)^2, \quad \text{(A18)}$$

and

$$r^* = \left(\frac{\gamma C_0 \nu \eta t}{kT}\right)^{1/2}. \tag{A19}$$

In the given case, q_i in eq (A11) equals 2 (Wagner, 1961).

A remarkable feature of surface- and supply-controlled Ostwald ripening is the evolution of the crystal size distribution with the passage of time. It was shown by Lifshitz and Slyozov (1961) and Wagner (1961) that at large time this distribution can be approximated by certain universal functions that develop irrespective of the initial CSD. For example, in the case of supply-controlled crystal growth this function has the form:

$$f(r, t) = \text{Const}\frac{(t^{-4/3})u^2}{(3 - 2u)^{11/3}(3 + u)^{7/3}} \exp\left(\frac{3}{2u - 3}\right), \tag{A20}$$

where $u = r/\bar{r} = r/r^*$. As can be seen in figure 9A, normalized $f(r, t)$ has an asymptotic profile with two characteristic features: (A) this function is equal or very close to zero at $u > 3/2$ or $r > (3/2)\bar{r}$; (B) it has a left-hand skewed distribution of crystal sizes.

Similar features are observed in the case of surface-controlled ripening:

$$f(r, t) = \text{Const}\frac{(t^{-2})u}{(2 - u)^5} \exp\left(\frac{3u}{u - 2}\right), \tag{A21}$$

where $u = r/r^*$ and $f(r, t) = 0$ for $u \geq 2$ (fig. 9B).

References

Anderson, T. F., and Chai, B. H. T., 1973, Oxygen isotope exchange between calcite and water under hydrothermal conditions, *in* Hofmann, A. W., Giletti, B. J., Yoder, H. S., Jr., and Yund, R. A., editors, Geochemical Transport and Kinetics: Carnegie Institute of Washington Publication 634, p. 219–227.

Baronnet, A., 1974, Étude en microscopie électronique des premiers stades de croissance d'un mica synthétique, la phlogopite hydroxylée. Phénomènes de coalescence et de murissement dans le système fermé conservatif: K_2O-6MgO-excès H_2O: High Temperatures-High Pressures, v. 6, p. 675–685.

—— 1982, Ostwald Ripening: The case of calcite and mica: Estudios Geologie, v. 38, p. 185–198.

Berner, R. A., 1981, Kinetics of weathering and diagenesis, *in* Lasaga, A. C., and Kirkpatrick, R. J., editors, Kinetics of Geochemical Processes: Mineralogical Society of America, Reviews in Mineralogy, v. 8, p. 111–134.

Carlson, W. D., Denison, C., and Ketcham, R. A., 1995, Controls on the nucleation and growth of porphyroblasts: kinetics from natural textures and numerical models: Geological Journal, v. 30, p. 207–225.

Cashman, K. V., and Ferry, J. M., 1988, Crystal size distribution (CSD) in rocks and the kinetics and dynamics of crystallization III. Metamorphic crystallization: Contributions to Mineralogy and Petrology, v. 99, p. 401–415.

Cashman, K. V., and Marsh, B. D., 1988, Crystal size distribution (CSD) in rocks and the kinetics and dynamics of crystallization II. Makaopuhi lava lake: Contributions to Mineralogy and Petrology, v. 99, p. 292–305.

Chai, B. H. T., 1973, Mass transfer of calcite during hydrothermal recrystallization, *in* Hofmann, A. W., Giletti, B. J., Yoder, H. S., Jr., and Yund, R. A., editors, Geochemical Transport and Kinetics: Carnegie Institute of Washington Publication 634, p. 205–218.

—— ms, 1975, The kinetics and mass transfer of calcite during hydrothermal recrystallization process: Ph.D. thesis, Yale University, 138 p.

Colbeck, S. C., 1986, Statistics of coarsening in water-saturated snow: Acta Metallurgica, v. 34, p. 347–352.

—— 1987, Theory of particle coarsening with a log-normal distribution: Acta Metallurgica, v. 35, p. 1583–1588.

Dowty, E., 1980, Crystal growth and nucleation theory and the numerical simulation of igneous crystallization, *in* Hargraves, R. B. editor, The Physics of Magmatic Processes: Princeton, Princeton University Press, p. 419–485.

Drits, V. A., Eberl, D. D., and Środoń, J., 1998, XRD measurement of mean thickness, thickness distribution and strain for illite and illite/smectite crystallites by the Bertaut-Warren-Averbach technique: Clays and Clay Minerals, v. 46, p. 461–475.

Eberl, D. D., Nüesch, R., Sucha, V., and Tsipursky, S., 1998, Measurement of fundamental illite particle thicknesses by X-ray diffraction using PVP-10 intercalation: Clays and Clay Minerals, v. 46, p. 89–97.

Eberl, D. D., and Środoń, J., 1988, Ostwald ripening and interparticle-diffraction effects for illite crystals: American Mineralogist, v. 73, p. 1335–1345.

Eberl, D. D., Środoń, J., Kralik, M., Taylor, B. E., and Peterman, Z. E., 1990, Ostwald ripening of clays and metamorphic minerals: Science, v. 248, p. 474–477.

Eberl, D. D., Środoń, J., Lee, M., Nadeau, P. H., and Northrop, H. R., 1987, Sericite from the Silverton caldera, Colorado: correlation among structure, composition, origin, and particle thickness: American Mineralogist, v. 72, p. 914–934.

Exner, H. E., and Lukas, H. L., 1971, The experimental verification of the stationary Wagner-Lifshitz distribution of coarse particles: Metallography, v. 4, p. 325–338.

Frost, H. J., and Thompson, C. V., 1987, The effect of nucleation conditions on the topology and geometry of two-dimensional grain structures: Acta Metallurgica, v. 35, p. 529–540.
Gabis, V., 1963, Étude minéralogique et géochimique de la série sédimentaire oligocène du Velay. Bulletin de la Société française de Minéralogie et de Cristallographie, v. 86, p. 315–354.
Garside, J., Phillips, V. R., and Shah, M. B., 1976, On size-dependent crystal growth: Industrial & Engineering Chemistry Fundamentals, v. 15, p. 230–233.
Gregg, J. M., Howard, S. A., and Mazzullo, S. J., 1992, Early diagenetic recrystallization of Holocene (<3000 years old) peritidal dolomites, Ambergris Cay, Belize: Sedimentology, v. 39, p. 143–160.
Inoue, A., and Kitagawa, R., 1994, Morphological characteristics of illitic clay minerals from a hydrothermal system: American Mineralogist, v. 79, p. 700–711.
Inoue, A., Velde, B., Meunier, A., and Touchard, G., 1988, Mechanism of illite formation during smectite to illite conversion in a hydrothermal system: American Mineralogist, v. 73, 1325–1334.
Jancic, S. J., Van Rosmalen, G. M., and Peeters, J. P., 1984, Growth dispersion in nearly monosize crystal populations, *in* Jancic, S. J. and deJong, E. J., editors, Proceedings 9th Symposium on Industrial Crystallization, Process Technology Proceedings, 2: New York, Elsevier, p. 43–49.
Joesten, R. L., 1991, Kinetics of coarsening and diffusion-controlled mineral growth, *in* Kerrick, D. M., editor, Contact Metamorphism: Mineralogical Society of America, Reviews in Mineralogy, p. 507–582.
Kapteyn, J. C., 1903, Skew Frequency Curves in Biology and Statistics: Groningen, Noordhoff, Astronomical Laboratory, 69 p.
Kerrick, D. M., Lasaga, A. C., and Raeburn, S. P., 1991, Kinetics of heterogeneous reactions, *in* Kerrick, D. M., editor, Contact Metamorphism: Mineralogical Society of America, Reviews in Mineralogy, p. 583–671.
Kirkpatrick, R. J., 1981, Kinetics of crystallization of igneous rocks, *in* Lasaga, A. C., and Kirkpatrick, R. J., editors, Kinetics of Geochemical Processes: Mineralogical Society of America, Reviews in Mineralogy, v. 8, p. 321–398.
Koch, A. L., 1966, The logarithm in biology I. Mechanisms generating the lognormal distribution exactly: Journal of Theoretical Biology, v. 12, p. 251–268.
—— 1969, The logarithm in biology II. Distributions simulating the lognormal: Journal of Theoretical Biology, v. 23, p. 276–290.
Kretz, R., 1966, Grain-size distribution for certain metamorphic minerals in relation to nucleation and growth: Journal of Geololgy, v. 74, p. 147–173.
Krumbein, W. C., and Graybill, F. A., 1965, An Introduction to Statistical Models in Geology: New York, McGraw-Hill Book Company, 475 p.
Larson, M. A., White, E. T., Ramanarayanan, K. A., and Berglund, K. A., 1985, Growth rate dispersion in MSMPR crystallizers: AlChE Journal, v. 31, p. 90–94.
Lasaga, A. C., 1981, Rate laws of chemical reactions, *in* Lasaga, A. C., and Kirkpatrick, R. J., editors, Kinetics of Geochemical Processes: Mineralogical Society of America, Reviews in Mineralogy, v. 8, p. 1–68.
—— 1982, Crystal growth from silicate melts: towards a master equation in crystal growth: American Journal of Science, v. 282, p. 1264–1288.
Lifshitz, I. M., and Slyozov, V. V., 1961, The kinetics of precipitation from supersaturated solid solutions: Journal of Physics and Chemistry of Solids, v. 19, p. 35–50.
Loveland, R. P., and Trivelli, P. H., 1947, Analysis of particle formation and growth by size-frequency determinations of the silver halide precipitations of photographic emulsions: Journal of Physical and Colloid Chemistry, v. 51, p. 1004–1027.
Mahin, K. W., Hanson, K., Morris, J. W. Jr., 1980, Comparative analysis of the cellular and Johnson-Mehl microstructures through computer simulation: Acta Metallurgica, v. 28, p. 443–453.
Markworth, A. L., 1970, The kinetic behavior of precipitate particles under Ostwald ripening conditions: Metallography, v. 3, p. 197–208.
Marsh, B. D., 1988, Crystal size distribution (CSD) in rocks and the kinetics and dynamics of crystallization I. Theory: Contributions to Mineralogy and Petrology, v. 99, p. 277–291.
Miyazaki, K., 1991, Ostwald ripening of garnet in high P/T metamorphic rocks: Contributions to Mineralogy and Petrology, v. 108, p. 118–128.
Morse, J. W., and Wang, Q., 1996, Factors influencing the grain size distribution of authigenic minerals: American Journal of Science, v. 296, p. 989–1003.
Mullin, J. W., 1974, Bulk crystallization, *in* Pamplin, B. R., editor, Crystal Growth (2nd edition): New York, Pergamon Press, p. 289–335.
Nadeau, P. H., Wilson, M. J., McHardy, W. J., and Tait, J. M., 1984, Interstratified clays as fundamental particles: Science, v. 225, p. 923–925.
Nielson, A. E., 1964, Kinetics of Precipitation: New York, Pergamon, 151 p.
Nordeng, S. H., and Sibley, D. F., 1996, A crystal growth equation for ancient dolomites: Evidence for millimeter-scale flux-limited growth: Journal of Sedimentary Research, v. 66, p. 477–481.
Ohara, M., and Reid, R. C., 1973, Modeling Crystal Growth Rates from Solution: Englewood Cliffs, New Jersey, Prentice-Hall, 272 p.
Randolph, A. D., and White, E. T., 1977, Modeling size dispersion in the prediction of crystal-size distribution: Chemical Engineering Science, v. 32, p. 1067–1076.
Randolph, A. D., and Larson, M. A., 1988, Theory of Particulate Processes, second edition: New York, Academic Press, 369 p.
Söhel, O., and Garside, J., 1992, Precipitation, Basic Principles and Industrial Applications: Boston, Butterworth-Heinemann Ltd., 391 p.
Środoń, J., Elsass, F., McHardy, W. J., and Morgan, D. J., 1992, Chemistry of illite/smectite inferred from TEM measurements of fundamental particles: Clay Minerals, v. 27, p. 137–158.

Stanton, R. L., and Gorman, H., 1968, A phenomenological study of grain boundary migration in some common sulfides: Economic Geology, v. 63, p. 907–923.
Vaz, M. F., and Fortes, M. A., 1988, Grain size distribution: the lognormal and the gamma distribution functions: Scripta Metallurgica, v. 22, p. 35–40.
Viczián, I., 1997, Hungarian investigations on the "Zempleni" illite: Clays and Clay Minerals, v. 45, p. 114–115.
Wagner, C., 1961, Theorie der Alterung von Neiderschlägen durch Umlösen (Ostwald Reifung): Zeitschrift fuer Elektrochemie, v. 65, p. 581–591.
Walton, A. G., 1967, The Formation and Properties of Precipitates: New York, Interscience Publishers, 232 p.
Weaire, D., Kermode, J. P., and Wejchert, J., 1986, On the distribution of cell areas in a Voronoi network: Philosophical Magazine B, v. 53, p. L101–L105.
White, E. T., and Wright, P. G., 1971, Magnitude of size dispersion effects in crystallization, *in* Larson, M. A., editor, Crystallization from solution: factors influencing size distribution: New York, American Institute of Chemical Engineers, p. 81–87.